Ore Geology Reviews 95 (2018) 695–712

Contents lists available at ScienceDirect

Ore Geology Reviews

journal homepage: www.elsevier.com/locate/oregeorev

Mineralogical constraints on the genesis of W–Nb–Ta mineralization in the Laiziling granite (Xianghualing district, south China)

Lei Xie[a,*], Zhengjun Wang[a], Rucheng Wang[a], Jinchu Zhu[a], Xudong Che[a], Jianfeng Gao[b], Xu Zhao[a]

[a] State Key Laboratory for Mineral Deposits Research, School of Earth Sciences and Engineering, Nanjing University, Nanjing 210023, China
[b] State Key Laboratory of Ore Deposit Geochemistry, Institute of Geochemistry, Chinese Academy of Sciences, Guiyang 550081, China

ARTICLE INFO

Keywords:
Wolframoixiolite
Qitianlinglite
Wolframite
Laiziling
Rare-metal granite

ABSTRACT

The Laiziling granitic pluton, located in the Xianghualing district, Hunan Province, China, comprises typical rare-metal granites with a pronounced vertical lithological zonation. This pluton includes three granitic phases comprising, from base to top, medium-grained (MG) alkali feldspar granite, fine-grained (FG) alkali feldspar granite and albite granite. Here we report the results of textural and chemical analyses of W–Nb–Ta oxide minerals from the Laiziling granitic pluton. The chemical compositions of whole-rock samples, rock-forming minerals and zircon have allowed us to identify the magmatic–hydrothermal processes that operated during the formation and rare-metal mineralization of the Laiziling pluton. The granites are slightly peraluminous to peraluminous, highly evolved and fractionated, as inferred from whole-rock geochemical and mineralogical (micas and zircon) signatures. All the micas in different granitic phases are classified into the zinnwaldite group. Li concentration in the primary micas (~2.6–4 wt% Li_2O) and Hf concentration (~1–8 wt% HfO_2) in the zircon increase for the base to the top granitic phases. Both alkali feldspar granites contain oxide mineral aggregates including columbite-group minerals, wolframoixiolite, qitianlingite, wolframite and cassiterite. The columbite-group minerals, wolframite and cassiterite also occur as isolated grains within the albite granite. The presence of the oxide minerals suggests that the W–Nb–Ta mineralization developed during the latter stages of the magmatic evolution, related to fluids that were compositionally evolved from the granites. The composition of the fluids controls the aggregate of the oxide minerals. The wolframite and cassiterite that precipitated within the Laiziling skarn-type deposit are chemically different from those within the granite, indicating a hydrothermal origin for the oxide minerals that formed as a result of pervasive alteration.

1. Introduction

The magmatic and hydrothermal systematics of rare-metal-bearing granites and the crystallization and precipitation of ore-bearing minerals have been investigated in numerous studies using natural samples (e.g., Cuney et al., 1992; Belkasmi et al., 2000; Smith et al., 2000; Van Lichtervelde et al., 2007; Galliski et al., 2008; Badanina et al., 2015) and high temperature–pressure (*T–P*) experimental studies (e.g., Linnen and Keppler, 1997; Linnen and Cuney, 2005; Borodulin et al., 2009; Che et al., 2013). These studies have highlighted that the texture and chemical composition of the ore-bearing oxide minerals (such as columbite-group minerals, cassiterite and wolframite) can be used to constrain the processes of rare-metal fractionation in granitic systems, including their magmatic–hydrothermal evolution and the concomitant migration and concentration of ore-forming elements (Černý et al., 1986; Tindle and Breaks, 2000; Huang et al., 2002; Wang et al., 2004). Some studies also have used rock-forming (micas) and accessory minerals (zircon) to better understand the processes of rare-metal fractionation (Raimbault and Burnol, 1998; Johan et al., 2012; Li and Huang, 2013; Breiter et al., 2014; Xie et al., 2016). As such, mineralogical studies have become an effective means of tracking magmatic–hydrothermal granitic systems and related rare-metal mineralization.

In the Xianghualing district of the Nanling Range, southern Hunan Province, there are W, Sn, Nb, Ta, Pb, Zn and fluorite deposits. In these deposits, ore minerals that are disseminated within the granite, as W–Sn-enriched skarn and hydrothermal bodies and as metasomatic deposits, together forming a polymetallic granitic and metallogenic series (Yuan et al., 2007). The Laiziling granitic pluton located within the Xianghualing district comprises typical rare-metal high-silica, high-alkalis, peraluminous granites that are enriched in volatiles, but depleted in Fe and Mg. A clearly defined zonation within the pluton is evident at outcrop scale, which comprises, from bottom to top, granite, greisen and pegmatite. Few comprehensive descriptions of the Laiziling

* Corresponding author.
E-mail address: xielei@nju.edu.cn (L. Xie).

https://doi.org/10.1016/j.oregeorev.2018.03.021
Received 26 December 2017; Received in revised form 23 March 2018; Accepted 23 March 2018
Available online 26 March 2018
0169-1368/

rare-metal granites and related deposits exist in the literature. Some studies have suggested that the polymetallic (W–Nb–Ta–Sn) mineralization is hosted within the Laiziling granite and greisen, and the skarn closed to the granite-country contact zone (Qiu et al., 2002; Zhu et al., 2011). Precise ages determined on zircon and biotite from the granite and cassiterite from the skarn demonstrate that magmatism and metallogenesis were contemporaneous at ca. 155 Ma (Hu et al., 1982; Yuan et al., 2008; Zhu et al., 2011). However, questions remain regarding the sequence of W–Nb–Ta mineralization, whether or not the disseminated wolframite and columbite formed throughout the magmatic to hydrothermal stage, and what factors controled variations in mineralization. Providing answers to these questions has significance for better understanding of the petrogenesis of W–Nb–Ta polymetallic mineralization in the Laiziling granitic pluton.

In this study, we use textural and chemical data for W–Nb–Ta oxide minerals, micas and zircon from the various petrographic phases identified within the Laiziling pluton. Combining with whole-rock analyses, we characterize the processes of magmatic fractionation and hydrothermal precipitation within the Laiziling granite, with implications for polymetallic mineralization.

2. Geological setting

The Nanling Range in southern China extends across four major metallogenic districts: Southern Jiangxi (Gan'nan), Southern Hunan (Xiang'nan), Northern Guangdong (Yue'Bei), and Northern Guangxi (Gui'bei) (Fig. 1a). Granite bodies of Yanshanian (Cretaceous–Jurassic) age make up ~30% of the exposed area (i.e. $> 64 \times 10^3$ km^2, Zhou et al., 2006), which are commonly associated with extensive Sn–W ± Nb ± Ta mineralization (Xu and Zhu, 1988; Hua and Mao, 1999; Hua et al., 2003).

The Xianghualing mining district is located to the south of Xianghualing town, ~20 km north of Linwu County, southern Hunan province (Xiang'nan ore district), in the central part of the Nanling Range, south China, which also includes well-known Qitianling, Yaogangxian, Qianlishan and Huashaping (Fig. 1b). The district is situated at the convergence of the NE-trending Chenzhou–Linwu Fault and the N–S-trending Leiyang–Linwu Fault (Wang et al., 1994). It comprises a tectono-magmatic anticlinal dome that is composed mainly of Paleozoic rocks with minor Mesozoic and Cenozoic strata. The main part of the lower Paleozoic sequence consists of Cambrian-aged strata dominated by arenaceous, argillaceous and siliceous rocks along with minor carbonates. The upper Paleozoic strata rest unconformably on the lower Paleozoic rocks, and are dominated by Middle Devonian conglomerates, sandstones and shales of the Tiaomajian Formation, Middle Devonian limestones and dolomites of the Qiziqiao Formation, Upper Devonian dolomitic limestones and sandstones of the Shetianqiao Formation and Carboniferous carbonates and clastic rocks (Yuan et al., 2008; Zhu et al., 2011; Huang et al., 2015).

The Laiziling pluton is located in the northeast of the Xianghualing district. It crops out over an area of 2.2 km^2, occurring as a northwestward elliptical granite stock (~2.4 km long and ~1 km wide), in which the peak of the dome is at an elevation of 1056 m (Fig. 1c). The pluton is a composite intrusive body exposing a variety of rock types. A characteristic feature of the pluton is a well-developed vertical zonation comprising, from bottom to top, the sequence 'protolithinoite' granite, two-mica granite and albite granite by petrographic observations (Qiu et al., 1998; Zhu et al., 2011). The main body of the Laiziling granite consists of zinnwaldite alkali feldspar granite (Zhao et al., 2008) or biotite granite (Yuan et al., 2007). The term 'protolithinoite', was used formerly to classify the presence of Li-rich micas, including zinnwaldite, Li-annite and Li-siderophyllite (Rieder et al., 1996). In this study, the micas present in all samples are classified as belonging to the zinnwaldite group, and the pluton is subdivided into three phases based on the varying abundance of K-feldspar and albite from the lower to upper parts of the pluton. These phases are: medium-grained alkali feldspar granite (hereafter MG alkali feldspar granite), which is dominated by K-feldspar; fine-grained alkali feldspar granite (hereafter FG alkali feldspar granite), which contains both K-feldspar and albite; and albite granite. In addition, four felsic dykes are found in the eastern and western parts of the Laiziling pluton. Among them, the longest dyke (No. 431) is ~1770 m long and 1.8 to 18 m wide, and consists of ongonite and topazite (Zhu et al., 2011; Huang et al., 2015).

Previous studies have recognized different types of mineralization and magmatic–hydrothermal deposits of various scales within the Laiziling pluton, including Nb–Ta mineralization related to the albite granite, W–Sn mineralization related to greisen and skarn and Nb–Ta–W–Sn hosted within the No. 431 dyke (Zhong and Li, 2006; Yuan et al., 2008; Zhu et al., 2011). However, the mineralization sequence and representative minerals for the rare metal mineralization are not well understood. Other types of mineralization include W–Sn–Be–F deposits in the skarn close to the granite–country rock contact zone, cassiterite–sulphide hyperthermal deposits in the outer contact zone and Pb–Zn deposits in the interlayered fracture zone within the wall rocks.

3. Sampling and analytical methods

In this study, we selected six samples of granite from the bottom to the top of the pluton. We also determined the whole-rock major and trace element compositions, and major and trace element mineral compositions, as detailed in the following sections.

Whole-rock major element compositions were measured using wet chemical analysis at the Analysis Center of the No. 230 Research Institute of the China National Nuclear Corporation (CNNC), Changsha, China. The procedures are described in the Chinese National standard protocol GB/T 14506-2010DZG93-05 (see Xie et al., 2015 for detailed information), for which all errors on the reported element concentrations are < 5% relative. The analyses of trace elements, including rare earth elements, were conducted with a PE Elan DRC-e ICP-MS at the State Key Laboratory of Ore Deposit Geochemistry, Institute of Geochemistry, Chinese Academy of Science, Guiyang, China. Rhodium was used as an internal standard to correct for matrix effects and instrument drift, which showed < 10% deviation from the recommended values for the international standards OU-6, AMH-1 and GBPG-1. Detailed information on the methods is presented in Qi et al. (2000).

Back-scattered electron (BSE) images and quantitative chemical analyses of minerals (feldspars, topaz, mica, zircon, Nb–Ta–W–Sn-bearing oxide minerals) were obtained on polished thin sections using a JEOL JXA-8100M electron microprobe (EMPA) at the State Key Laboratory for Mineral Deposits Research at Nanjing University, China. The operating conditions were set at an acceleration voltage of 15 kV, a probe current of 20nA for all elements and a beam diameter of 4 μm for micas and feldspars and 1 μm for other minerals. The peak counting times for the major and the minor elements were 10 s and 20 s, respectively. The major elements determined were Si, Al, Na and K for feldspar; Si, Al and F for topaz; Si, Al, Fe, K and F for mica; Si, Zr and Hf for zircon; Nb, Ta, Mn, Fe and W for columbite group minerals, wolframoixiolite and qitianlingite; W, Mn and Fe for wolframite; and Sn, Fe and Mn for cassiterite. The elements Si, Al, Na, Mg and Rb were determined by the crystal TAP; the element F was determined by the crystal LDE; the elements P, K, Ca, Sc, Ti, Y, Zr, Nb, Sn, Th and U were determined by the crystal PET; and the elements Mn, Fe, Hf, Ta, and W were determined by the crystal LIF. All data were corrected using standard ZAF correction procedures. Natural minerals (fayalite, orthoclase, topaz and hornblende) were used as standards for silicate mineral analysis, while natural minerals (fayalite and scheelite), synthetic metals (Nb, Ta and Sc metals), and synthetic compounds (SnO_2 and $MnTiO_3$) were used as standards for oxide mineral analysis.

In situ analyses of micas and K-feldspar for 42 elements were conducted by laser ablation–inductively coupled plasma–mass spectrometry (LA–ICP–MS) at Nanjing FocuMS Technology, Nanjing, China. A

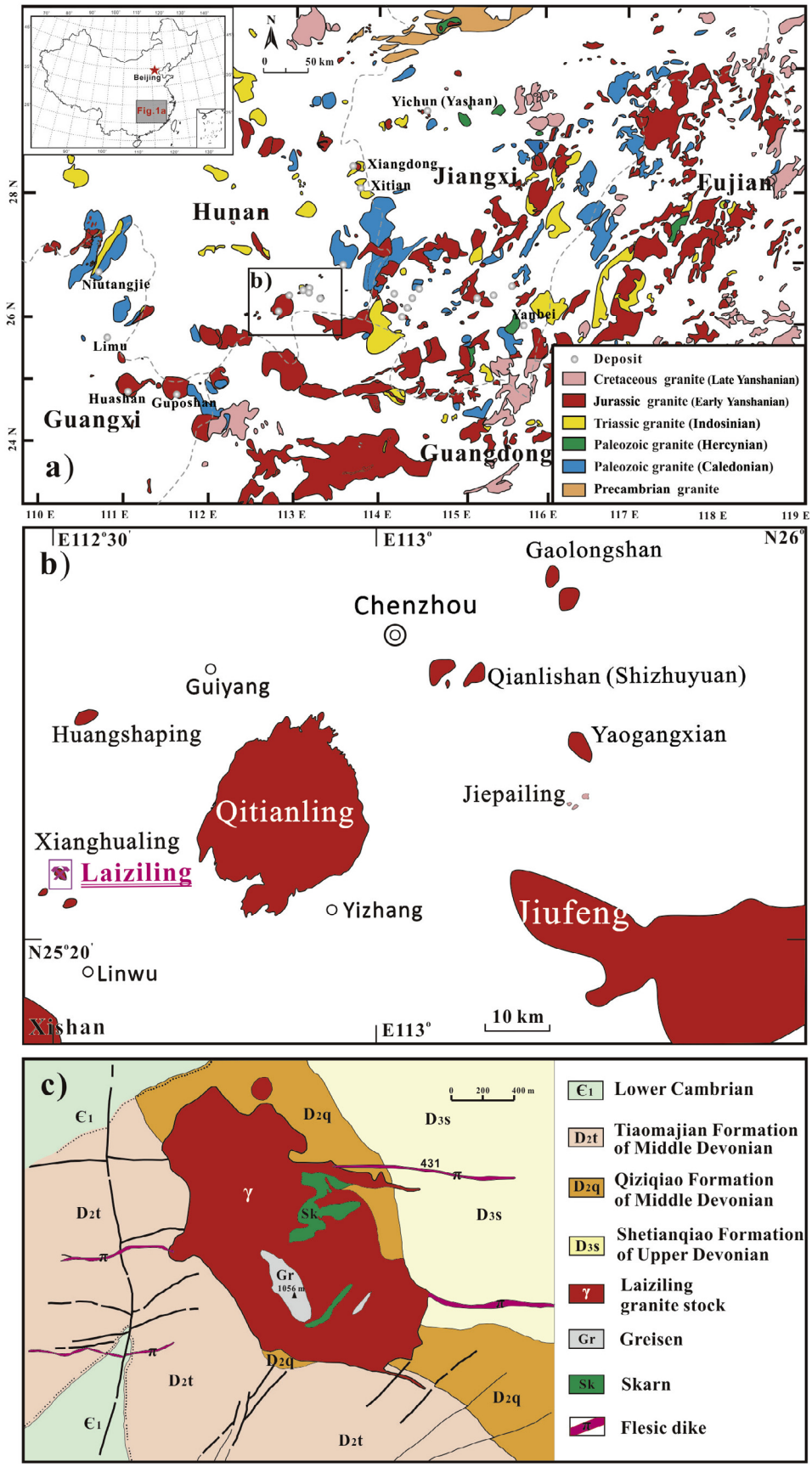

Fig. 1. (a) Distribution of granites and rare-metal deposits in the Nanling and adjacent range, south China (Sun, 2006); (b) geological map of the Xiang'nan ore district (south Hunan province); and (c) geological map of Laiziling granite in Xianghualing district. Modified after Zhu et al. (2011).

PhotonMachines Excite laser ablation system (Lamda Physik, Gottingen, Germany) integrated with an ICP–MS (Agilent 7700x, Agilent Technologies, Tokyo, Japan) were used for the analyses. The 193 nm ArF excimer laser, homogenized by a set of beam delivery systems, was focused on mineral surfaces with fluence of 10 J/cm^2. The ablation protocol employed a spot diameter of 44 μm at a repetition rate of 4 Hz (for micas) and 5 Hz (for K-feldspar) for 40 s (equating to 160 pulses). Helium was applied as the carrier gas to efficiently transport aerosol to the ICP–MS. The following isotopes were measured: ^{7}Li, ^{25}Mg, ^{27}Al, ^{29}Si, ^{44}Ca, ^{45}Sc, ^{49}Ti, ^{51}V, ^{53}Cr, ^{55}Mn, ^{57}Fe, ^{59}Co, ^{60}Ni, ^{85}Rb, ^{88}Sr, ^{89}Y, ^{90}Zr, ^{93}Nb, ^{95}Mo, ^{118}Sn, ^{133}Cs, ^{137}Ba, ^{139}La, ^{140}Ce, ^{141}Pr, ^{146}Nd, ^{147}Sm, ^{151}Eu, ^{155}Gd, ^{159}Tb, ^{163}Dy, ^{165}Ho, ^{167}Er, ^{169}Tm, ^{173}Yb, ^{175}Lu, ^{178}Hf, ^{181}Ta, ^{182}W, ^{208}Pb, ^{232}Th and ^{238}U. United States Geological Survey basaltic glasses (BIR-1G, BHVO-2G, BCR-2G and GSE-1G) were analysed for external calibration (Gao et al., 2013). Chinese Geological Standard Glasses (CGSG-1, CGSG-2, CGSG-4 and CGSG-5), prepared by the National Research Center for Geoanalysis, Beijing, China, were analysed for quality control (Hu et al., 2011). ^{29}Si was used as an internal standard. Off-line data processing was performed using the ICPMSDataCal program (Liu et al., 2008). The estimated precision is better than ± 5% for major elements and ± 10% for trace elements.

The Li concentration determined by LA–ICP–MS should be viewed with caution on account of the low precision. However, a good positive linear correlation exists between Li determined by LA–ICP–MS and SiO_2 determined by EMPA for Fe-rich mica, so the Li concentration was also calculated according to the empirical methods proposed by Monier and Robert (1986) for muscovite and Tindle and Webb (1990) for Fe-rich mica. The good positive linear correlation between Li determined by LA–ICP–MS and Li calculated according to the empirical method suggests both methods can be relied upon for determining the Li concentration of mica.

4. Results

4.1. Petrography and geochemistry of the Laiziling granite

The three different phases of the pluton have similar textures, although the abundance of minerals is variable. The MG alkali feldspar granite has a subhedral-granular medium-grained texture transitional to seriate texture with a grain size of 1–5 mm (Fig. 2a, b). The main rock-forming minerals consist of quartz (40–45 vol%), K-feldspar (25–30%, occasionally occurring as perthite), and albite (20–25%). Zinnwaldite concentrations vary between 4 and 8 vol% and is partially altered to muscovite at its margins and along cleavage planes (Fig. 2c). Micas occur as flakes of 1–2 mm in interstitial positions between feldspars and quartz and commonly contain inclusions of fluorite and zircon. Topaz is commonly subhedral with well-developed terminations and prism faces in larger grains (> 100 μm), present as a minor mineral within interstices between major minerals in the MG alkali feldspar granite (Fig. 2d). From the MG alkali feldspar granite, through the FG alkali feldspar granite to the albite granite, the abundance of K-feldspar decreases whilst that of albite increases sharply. The FG alkali feldspar granite has a grain size of 0.2–1 mm, and comprises mainly quartz (40 vol%), albite (25–28%), K-feldspar (25–30%), zinnwaldite (5%) and topaz (1–2%)(Fig. 2e, f). The albite granite, which is exposed at the top of the Laiziling granitic pluton, is distinguished by colour in white and fine-grained porphyritic-like texture from the alkali-feldspar granites. It consists predominantly of tabular albite (30–40 vol%), quartz (40%) and zinnwaldite (5–15%) (Fig. 2g, h) with minor K-feldspar (2–8%) and topaz. Topaz in the albite granite is < 50 μm across, and present dominantly as anhedral grains that are intergrown with the other main rock-forming minerals. The abundance of topaz grain varies in the two studied albite granite samples, rare in one sample (15LZL07) and up to 8% in another sample (15LZL13). The quartz phenocrysts contain abundant inclusions of albite laths without concentric arrangement, similar to the so-called “snowball quartz” texture.

The whole-rock chemical compositions of the Laiziling granites are given in Table 1. The MG alkali feldspar and FG alkali feldspar granites have similar chemical compositions, whereas the two albite granites differ, largely due to variations in the abundance of topaz. The compositional characteristics of the granites can be summarized as follows: (1) The granites are characterized by relatively high SiO_2 (~77 wt% in the alkali feldspar granites and ~75 wt% in the albite granite) and Al_2O_3 (ranging from 11.9 to 12.6 wt% in the alkali feldspar granites, increasing sharply to ~17 wt% in the topaz-bearing albite granite). All samples are weakly peraluminous to peraluminous. (2) The granites contain intermediate concentrations of alkali elements, with K_2O + Na_2O contents varying from 5.7 to 7.8 wt% (i.e., the rocks are subalkaline). The alkali feldspar granites have similar K_2O/Na_2O ratios (averages of 1.5 and 1.4, respectively), which are higher than the albite granite (~0.64). (3) The granites have low concentrations of MgO, TiO_2 and MnO (< 0.1 wt%); CaO contents in the albite granite (as low as 0.02 wt%) are lower than those of the alkali feldspar granites (average of 0.5 wt%). (4) The topaz-bearing albite granite has extremely high F contents of ~3 wt%.

Granites have similar chondrite-normalized rare earth element (REE) patterns, with fractionated arrays (La_N/Yb_N ratios averaging at 2.3) and strong negative Eu anomalies (Eu/Eu∗ values = 0.01 and 0.3 for topaz-rich albite granite) (Fig. 3, Table 1). Total REE concentrations decrease from the alkali feldspar granites (averaging at 252 ppm) to the albite granite (as low as 62 ppm) (Table 1). Both types of alkali feldspar granites are characterized by flat heavy REE patterns (Gd_N/Yb_N ratios averaging at ~0.75), while the albite granite shows a moderately positive heavy REE pattern (Gd_N/Yb_N ratios averaging at ~0.48). The alkali feldspar granites contain Zr (~92 ppm on average), Hf (~5 ppm), Th(~34 ppm) and U(~29 ppm), whereas the Zr content of the albite granite (~43 ppm) is relatively low. Zr/Hf ratios decrease significantly from ~ 17 to 9 from the alkali feldspar granites to albite granites. The variation trends of Sr concentrations are similar, decreasing from alkaline granites (~8.5 ppm) to the albite granite (~5 ppm). The albite granite has higher contents of Nb + Ta (up to 134 ppm) and lower Nb/Ta ratios (1.9) than the alkali feldspar granites (~74 ppm and ~4.8, respectively). The albite granite is particularly rich in W (up to 103 ppm).

4.2. Mineral chemistry of rock-forming minerals

4.2.1. Feldspars

K-feldspar and albite in the Laiziling granite are close to pure end-member compositions (Table 2). K-feldspar has a low proportion of albite (< 2.8 mol.%), and albite contains an orthoclase content of only 1.8 mol.%. All feldspars have very low anorthite contents (< 0.2 mol.%). K-feldspars from different samples have increasing Rb concentration from ~3000 ppm in the alkali feldspar granite to ~4000 ppm in the albite granite and slightly decreased K_2O/Rb_2O ratios from 50 to 37. The Cs concentrations in the K-feldspar are as low as 30 ppm.

4.2.2. Topaz

EMPA results indicate that the topaz in the Laiziling granite is similar, mainly containing SiO_2 (~33 wt%), Al_2O_3 (55–57 wt%) and F (17.3 to 20.2 wt%). They are all closed to the fluorine-dominated end member. The other oxides analyzed in the topaz are all < 0.1 wt% (Table 3).

4.2.3. Micas

Micas occur in various grain sizes ranging from 20 to 1000 μm, and are present in all granitic samples. Most grains are compositionally homogeneous and classified as belonging to the zinnwaldite group, although some grains from the MG alkali feldspar granite are partially altered to muscovite at their margins and along cleavage planes (Figs. 2c and 4a–b). Compositionally, from the MG alkali feldspar

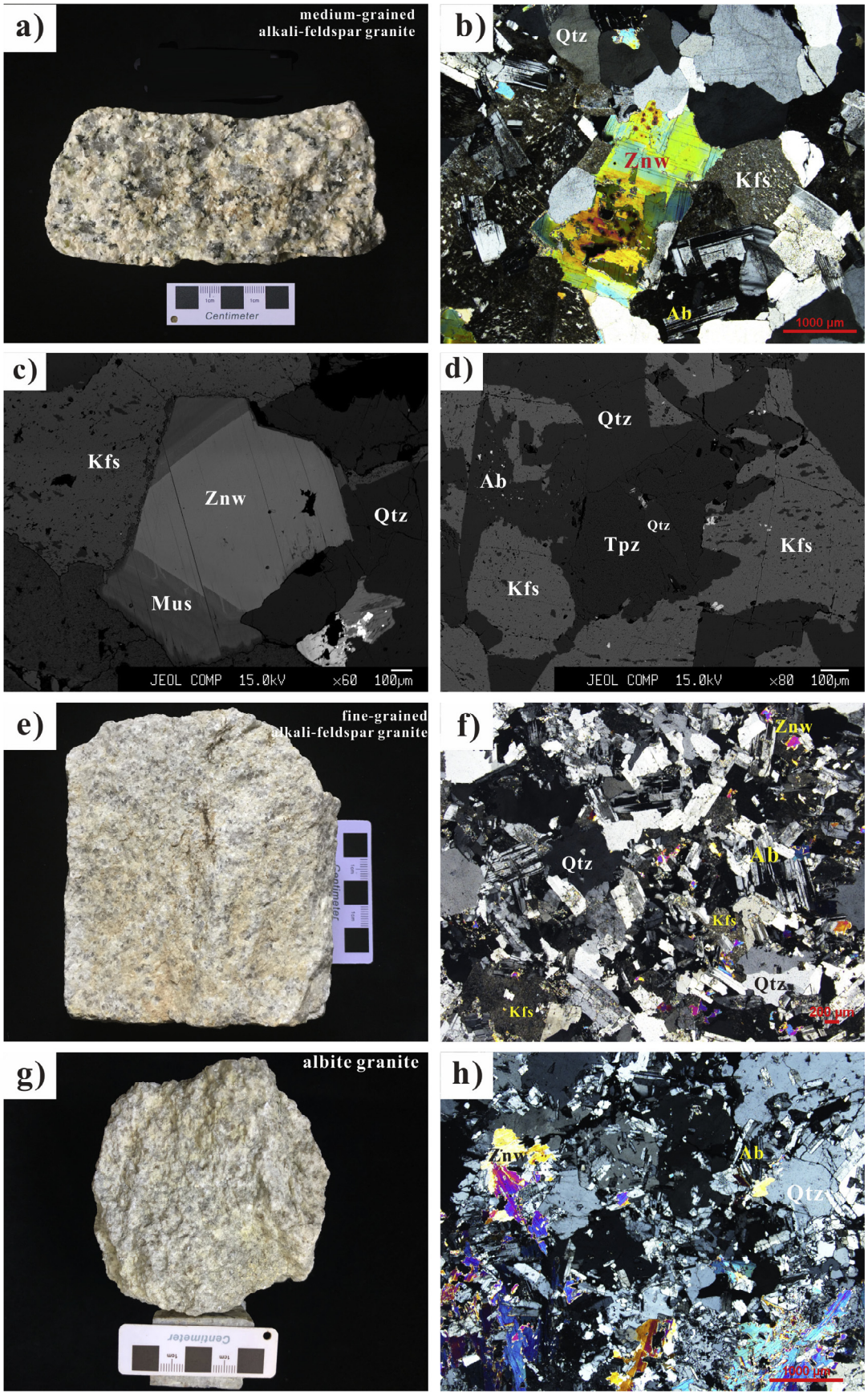

Fig. 2. Hand specimen photographs and photomicrographs showing the petrographic characteristics of the Laiziling samples: (a) hand specimen of the medium-grained alkali feldspar granite; (b) abundant perthite dominates feldspars within the medium-grained alkali feldspar granite; (c) BSE images of zoned zinnwaldite in the alkali feldspar granite; (e) and (f) fine-grained alkaline feldspar granite containing K-feldspar and albite grains; (g) and (h) albite granite with 'snowball-like' texture in the bottom-right of the image. Mineral abbreviations: Kfs – K-feldspar; Ab – albite; Qtz – quartz; Tpz – topaz; Znw – zinnwaldite; Mus –muscovite.

Table 1
Major- and trace-element compositions of the Laiziling granite.

	MG alkali- feldspar granite		FG alkali-feldspar granite		Albite granite			MG alkali- feldspar granite		FG alkali-feldspar granite		Albite granite	
15LZL-	05	17	03	21	07	13		05	17	03	21	07	13
SiO_2 (wt.%)	76.93	77.06	77.34	76.46	78.18	70.99	Sn (ppm)	29	19	22	22	13	42
TiO_2	0.04	0.03	0.04	0.03	0.01	0.01	W	37	16	46	27	96	103
Al_2O_3	12.62	12.24	11.92	12.54	12.39	16.52	Th	35	34	33	34	17	5.8
Fe_2O_3	0.32	0.36	0.32	0.33	0.19	0.69	U	27	30	27	30	25	3.8
FeO	0.73	1.12	0.62	0.73	0.11	2.03	Cr	2.8	3.4	5	2.4	2.7	4.6
MnO	0.07	0.16	0.06	0.09	0.04	0.38	V	0.26	0.2	0.85	0.36	0.27	0.09
MgO	0.06	0.06	0.09	0.05	0.02	0.07	Pb	49	113	50	745	41	36
CaO	0.57	0.45	0.49	0.50	0.32	0.02	Co	0.22	0.10	0.29	0.08	0.00	0.24
Na_2O	3.43	2.49	3.19	3.05	4.75	3.44	Ga	28	26	26	25	34	43
K_2O	4.18	4.57	4.20	4.60	3.03	2.24	Mo	0.25	18	1.8	1.9	2.0	8.3
P_2O_5	0.01	0.01	0.01	0.01	0.01	0.01	Rb/Sr	150	194	143	241	159	550
LOI	1.12	1.30	1.02	1.00	0.82	2.26	Zr/Hf	17.0	16.3	18.1	16.2	9.2	8.1
F	0.65	0.96	0.65	0.89	0.32	3.00	Nb/Ta	3.93	5.08	4.57	5.50	2.12	1.85
Total	100.07	99.85	99.31	99.39	99.87	99.02	Th/U	1.30	1.13	1.22	1.13	0.68	1.51
Na_2O+K_2O	7.61	7.06	7.39	7.65	7.78	5.68							
K_2O/Na_2O	1.22	1.84	1.32	1.51	0.64	0.65	La (ppm)	43	39	35	39	23	11
A/CNK	1.13	1.24	1.12	1.15	1.06	2.04	Ce	95	92	80	91	54	24
A/NK	1.24	1.35	1.22	1.25	1.12	2.05	Pr	12	11	10	11	6.5	3.9
FeO_t/MgO	16.97	24.07	10.09	20.54	14.05	36.33	Nd	42	39	34	39	18	10
							Sm	12	12	10	12	5.0	2.6
Be(ppm)	6.2	4.1	14	4.9	4.7	10	Eu	0.04	0.04	0.04	0.05	0.01	0.21
Li	585	959	577	624	302	2576	Gd	12	11	10	12	4.3	1.6
Rb	1351	1709	1357	1443	1015	2121	Tb	2.7	2.3	2.4	2.5	0.99	0.37
Cs	47	71	48	53	14	67	Dy	19	16	17	18	6.8	2.4
Sr	9.0	8.8	9.5	6.0	6.4	3.9	Ho	3.9	3.3	3.5	3.6	1.4	0.44
Ba	20	8.7	30	5.7	4.7	6.2	Er	12	9.8	11	11	4.8	1.5
Sc	6.5	4.5	6.7	4.5	5.4	5.6	Tm	2.1	1.6	1.9	1.8	0.96	0.31
Y	115	87	106	98	26	7.6	Yb	15	10	14	13	7.6	2.7
Zr	102	88	98	81	47	39	Lu	2.1	1.4	1.9	1.8	1.1	0.40
Hf	6	5.4	5.4	5	5.1	4.9	ΣREE	273.07	248.44	230.74	255.75	134.46	61.95
Nb	59	66	64	55	91	64	LREE/ HREE	2.96	3.48	2.74	3.01	3.81	5.35
Ta	15	13	14	10	43	34	δEu	0.01	0.01	0.01	0.01	0.01	0.30

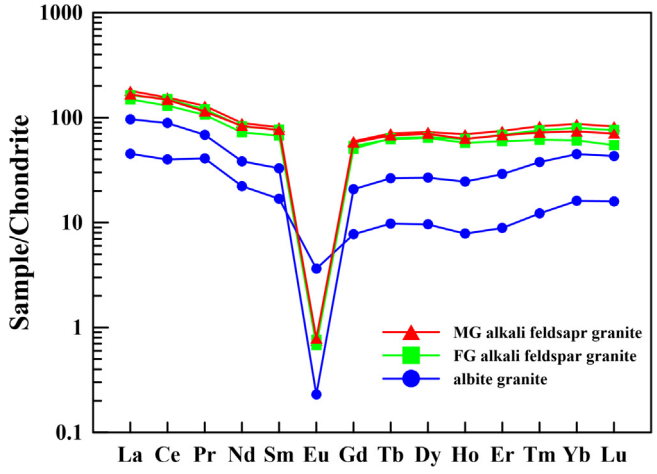

Fig. 3. Chondrite-normalized REE patterns of sample from the Laiziling granite. Chondrite REE values are from Sun and McDonough (1989).

granite though the FG alkali feldspar granite to the albite granite, the micas show a gradual increase in Li_2O (on average, 2.8, 2.9 and 3.3 wt %, respectively), F (on average, 8.8, 9.1 and 9.9 wt%, respectively) and MnO contents (on average, 1.1, 1.3 and 1.9 wt%, respectively) (Table 4), and a gradual decrease in Al and Fe contents (Fig. 4c). The zinnwaldites from different samples have similar K_2O and Rb_2O contents, and K_2O/Rb_2O ratios, in which Rb_2O contents are up to 1.36 wt% (Fig. 4d). The TiO_2 (< 0.6 wt%), MgO (< 0.1 wt%), CaO (< 0.1 wt%) and Na_2O (< 0.1 wt%) contents are relatively low in all zinnwaldite grains.

LA–ICP–MS analyses indicate that zinnwaldites within the Laiziling granite are rich in Nb, Ta, W and Sn, but exhibit considerable compositional variation between the different samples (Table 4). The Ta content increases gradually (on average, 40, 56 and 88 ppm, respectively) from the MG alkali feldspar granite, through the FG alkali feldspar granite to the albite granite, and the Nb/Ta ratio decreases concomitantly (Fig. 4e). Zinnwaldites are relatively rich in Sn in the MG and FG alkali feldspar granites, whereas the albite granite is enriched in W (Fig. 4f).

4.3. Oxide minerals

The Nb–Ta–W–Sn oxide minerals in the Laiziling granite include accessory columbite-group minerals, wolframoixiolite, qitianlingite, wolframite and cassiterite (Figs. 5 and 6a). Within the alkali feldspar granites, these oxide minerals are generally present as complex anhedral grain aggregates 100–300 μm across that occur within the interstices between rock-forming minerals (Fig. 5a–f). A clear overgrowth sequence characterizes these aggregates, which comprise, from core to rim: columbite-group minerals, wolframoixiolite [with the general formula $(Nb,Ta,W,Fe,Mn,Ti,Sn)_4O_8$], qitianlingite [$(Fe,Mn)_2(Nb,Ta)_2WO_{10}$, only in the FG alkali feldspar granite], wolframite and subhedral cassiterite. The mineral aggregates may also contain quartz and calcite. Within the albite granite, disseminated oxide minerals (columbite-group minerals, wolframite and cassiterite) are commonly present as isolated grains (Fig. 5g–h).

4.3.1. Columbite-group minerals

As described above, columbite-group minerals within the alkali feldspar granites generally form aggregates with other oxide minerals. In all samples in which they occur, the columbite-group minerals have similar crystal morphologies and chemical compositions, and mostly occur as subhedral to anhedral crystals exhibiting oscillatory zonation.

Table 2
Representative chemical results of feldspars in the Laiziling granite.

	MG alkali-feldspar granite				FG alkali-feldspar granite				Albite granite			
	K-feldspar		Albite		K-feldspar		Albite		K-feldspar		Albite	
	1	2 average (n = 7)	3	4	5	6 average (n = 9)	7	8	9	10 average (n = 12)	11	12
SiO_2 (wt.%)	63.73	64.24	67.43	67.74	63.49	64.05	69.39	68.90	64.83	64.61	67.86	70.32
TiO_2	0.04	0.04	0.03	0.03	0.10	0.07	0.08	0.02	0.07	0.07	0.05	0.03
Al_2O_3	17.43	17.82	19.46	19.48	18.10	17.86	19.52	19.31	18.00	18.01	18.77	19.57
CaO	0.02	0.01	0.02	0.14	0.01	0.02	0.03	0.01	–	0.00	0.01	0.07
FeO	–	0.02	–	0.03	0.01	0.00	0.06	0.05	0.03	0.03	0.04	0.01
Na_2O	0.13	0.17	11.11	10.44	0.30	0.22	11.05	11.39	0.21	0.16	10.93	10.75
K_2O	15.73	15.97	0.30	0.29	15.39	16.16	0.25	0.23	15.87	15.88	0.22	0.25
Rb_2O*	n.a.	0.32	n.a.	n.a.	n.a.	0.33	n.a.	n.a.	n.a.	0.43	n.a.	n.a.
Cs* (ppm)	n.a.	28	n.a.	n.a.	n.a.	31	n.a.	n.a.	n.a.	31	n.a.	n.a.
Total	97.08	98.58	98.35	98.20	97.40	98.72	100.39	99.91	99.01	99.19	97.89	101.02
K_2O/Rb_2O		50				49				37		
An	0.09	0.05	0.09	0.72	0.07	0.08	0.13	0.07		0.01	0.04	0.37
Ab	1.24	1.54	98.15	97.51	2.83	2.07	98.38	98.63	1.95	1.53	98.63	98.14
Or	98.67	98.41	1.76	1.77	97.11	97.86	1.48	1.30	98.05	98.46	1.33	1.49

-: below detection limits.
n.a.: not analyzed.
*: Rb and Cs are determined by LA-ICP-MS.

Individual grains are 2–10 μm across and always show the darkest BSE response within the complex oxide assemblage (Fig. 5b, d). Compositionally, Ta# [Ta/(Nb + Ta)] shows little variation (average of 0.19), whereas Mn# [Mn/(Fe + Mn)] ranges from 0.3 to 0.6, and the columbite-group minerals are classified as ferrocolumbite and manganocolumbite (Table 5; Fig. 6b). Of particular note are the relatively high WO_3 concentrations (~5–15 wt%) within the columbite-group minerals.

Columbite-group minerals within the albite granite are different from those within the alkali feldspar granites. They are generally present as euhedral to subhedral crystals 20–100 μm across that are intergrown with wolframite (Fig. 5g–h). Gradual variations in the compositions of the columbite-group minerals are evident in the changing BSE response that varies from dark to bright from core to rim. Individual grains have consistent Mn# values (~0.51), but Ta# values that increase from the core (0.13 on average) to rim (0.25 on average) (Table 5; Fig. 6c). The columbite-group minerals within the albite granite have lower WO_3 concentrations (average of 3.2 wt%) and higher Nb_2O_5 + Ta_2O_5 concentrations (~73 wt%) compared with those from the alkali feldspar granites.

4.3.2. Wolframoixiolite

Wolframoixiolite is absent in the albite granite but present in both types of alkali feldspar granite as anhedral crystals ~5 μm in size that show patchy and "symplektitic-like" textures (Fig. 5b, d, f). Wolframoixiolite grains generally have a brighter BSE response than the columbite-group minerals that they are intergrown with, and occupy the bulk of the aggregate. Compositionally, the wolframoixiolite grains contain on average WO_3 ~ 22 wt%, Nb_2O_5 + Ta_2O_5 ~ 55 wt%, FeO + MnO ~ 20 wt% and SnO_2 ~ 1.4 wt%, and have Ta# ~ 0.22 and Mn# ~ 0.54 (Table 6; Fig. 6a–b). It is difficult to distinguish the various oxide minerals from each other on the basis of their BSE response, but they could be confirmed by the elements (W, Nb, Ta and Sn) X-ray scanning mappings (Fig. 5a).

4.3.3. Qitianlingite

Qitianlingite occurs only in the oxide assemblage within the FG alkali feldspar granite (Fig. 5d, f). Compositionally, they are characterized by extremely high WO_3 concentrations, up to 40 wt% with an average of 29 wt%, equating to 0.86 atoms per formula unit (apfu) calculated on a 10 oxygen basis (Table 6; Fig. 6a). The ranges of Ta# and Mn# values (on average 0.22 and 0.57, respectively) within qitianlingites are close to those within the Nb–Ta oxide intergrowths, such as the columbite-group minerals and wolframoixiolites.

4.3.4. Wolframite

Wolframite grains within the alkali feldspar granites are mostly present as anhedral crystals 1–50 μm wide that are included in the

Table 3
Representative electron-microprobe results of topaz in the Laiziling granite.

	MG alkali-feldspar granite			FG alkali-feldspar granite			Albite granite		
	1	2	3	4	5	6	7	8	9
SiO_2 (wt.%)	33.39	33.37	34.09	33.40	32.63	33.03	32.91	33.56	33.33
TiO_2	–	0.01	0.03	0.01	0.01	0.03	–	–	–
Al_2O_3	56.04	55.79	55.38	56.25	56.02	55.97	56.75	55.81	55.15
MgO	0.01	0.02	–	0.00	0.02	–	–	0.01	–
CaO	0.02	0.02	0.00	0.01	0.04	0.00	0.01	–	0.01
MnO	0.01	0.04	–	0.01	–	0.01	–	–	0.03
FeO	0.02	0.02	–	0.02	0.02	0.03	0.02	0.04	0.00
Na_2O	0.03	0.02	–	0.01	0.02	0.02	–	–	–
K_2O	0.02	–	0.01	0.01	0.00	0.01	0.01	0.01	0.01
F	17.81	17.36	19.03	18.15	17.30	18.06	18.70	18.55	18.35
F = O	7.50	7.31	8.01	7.64	7.28	7.60	7.87	7.81	7.73
Total	99.85	99.33	100.53	100.23	98.77	99.54	100.53	100.17	99.16

Table 4
Representative EPMA and LA-ICPMS analyses data for the micas of the Laiziling granite.

	MG alkali-feldspar granite						FG alkali-feldspar granite				Albite granite			
	Zinnwaldite				Muscovite		Zinnwaldite				Zinnwaldite			
	1	2	3	4	5	6	7	8	9	10	11	12	13	14
EPMA (wt.%)														
SiO_2	44.65	43.16	42.19	42.73	50.15	50.19	43.75	42.80	43.97	42.22	44.27	44.00	44.00	45.66
TiO_2	0.17	0.16	0.15	0.12	0.15	0.05	0.19	0.16	0.24	0.21	0.12	0.20	0.18	0.14
Al_2O_3	21.28	21.99	22.01	21.59	30.72	30.47	21.56	21.54	21.39	21.85	21.49	21.58	21.75	21.20
FeO	14.58	15.14	15.95	15.27	6.13	6.82	15.43	15.52	14.62	15.81	13.13	12.82	13.33	12.55
MnO	1.05	1.14	1.53	1.46	0.16	0.17	1.09	1.04	1.09	1.41	2.07	2.00	2.11	1.29
MgO	0.01	0.02	0.02	0.04	–	0.03	0.03	0.03	0.05	0.03	–	0.02	0.04	–
CaO	–	–	–	–	–	–	–	–	0.01	–	–	0.02	–	–
Na_2O	0.03	–	–	–	–	0.02	0.02	–	0.01	0.02	–	–	0.01	–
K_2O	9.43	9.10	9.08	9.19	8.13	7.75	9.23	9.37	9.36	9.20	9.35	9.15	9.26	9.54
F	8.64	9.86	9.15	9.48	1.60	1.53	8.36	8.94	9.54	9.12	10.10	10.34	10.12	10.22
Li_2O^*	3.26	2.83	2.56	2.71	0.42	0.40	3.00	2.73	3.07	2.57	3.15	3.07	3.08	3.55
H_2O^*	0.07	0.00	0.00	0.00	3.77	3.80	0.17	0.00	0.00	0.00	0.00	0.00	0.00	0.00
O = F, Cl	3.64	4.15	3.85	3.99	0.67	0.64	3.52	3.76	4.02	3.84	4.25	4.35	4.26	4.30
Total	99.53	99.26	98.77	98.60	100.56	100.58	99.31	98.36	99.34	98.60	99.42	98.85	99.60	99.84
LA-ICP-MS (wt.%)														
Li_2O	2.55	2.89	2.67	2.95	0.24	0.18	2.95	2.64	2.90	2.64	3.29	3.33	3.08	3.38
Rb_2O	1.19	1.20	1.25	1.28	0.42	0.35	1.26	1.19	1.27	1.18	1.25	1.23	1.21	1.36
Cs_2O	0.07	0.09	0.08	0.09	0.03	0.02	0.09	0.09	0.11	0.08	0.04	0.03	0.03	0.04
LA-ICP-MS (ppm)														
Sc	51	39	35	34	15	14	38	40	31	28	33	35	31	48
V	11	1.8	2.1	2.0	1.3	1.4	1.5	1.4	0.91	2.0	0.88	0.76	0.98	0.85
Ga	140	85	110	115	126	94	116	140	114	113	81	69	73	82
Ge	8.6	6.3	6.8	4.5	4.3	4.6	4.0	–	5.8	5.0	5.9	4.8	3.1	6.0
Sr	0.52	–	0.15	–	0.32	0.30	0.08	0.12	0.15	0.14	0.16	0.74	0.28	0.04
Y	0.31	–	0.08	0.01	–	0.03	0.04	0.57	0.13	0.56	0.07	0.72	0.39	–
Zr	0.33	–	0.14	0.19	0.19	0.11	0.12	0.14	0.23	0.31	0.09	0.33	0.25	0.26
Nb	122	166	395	169	12	13	158	217	271	356	269	217	251	257
Mo	0.42	0.38	0.49	0.61	–	0.30	0.49	0.24	0.40	0.81	0.64	0.46	0.55	0.48
In	1.3	1.4	1.6	1.3	3.2	2.8	1.5	1.3	2.2	1.6	1.2	0.95	1.1	1.0
Sn	188	162	271	168	632	589	221	232	243	196	126	79	93	121
Ba	12	2.7	3.6	2.5	2.5	2.3	6.2	2.8	5.1	5.2	2.9	4.4	3.1	2.8
Hf	–	0.11	0.17	0.13	–	0.09	0.05	0.02	–	0.08	–	0.05	–	0.20
Ta	11	23	79	30	7.7	8.0	22	30	62	67	109	126	112	152
W	33	34	31	21	4.6	4.2	18	20	28	28	58	60	59	57
Tl	38	33	38	41	18	17	39	39	39	37	30	30	28	33
Pb	9.2	4.2	5.3	5.6	0.56	0.93	7.0	8.0	5.9	7.2	3.9	7.3	6.0	3.9
Th	0.22	0.01	0.04	–	0.04	–	0.01	0.06	0.37	0.15	0.04	0.05	–	–
U	1.71	0.05	0.10	–	–	–	0.05	0.35	0.44	0.37	0.04	0.12	0.07	–

*: Li_2O and H_2O calculation are after Tindle and Webb (1990) and Monier and Robert (1986).

oxide mineral aggregates (Fig. 5a–f). They are homogeneous and contain minor Nb_2O_5 + Ta_2O_5 (averaging 5 wt%) concentrations, and Ta# and Mn# values close to those of the Nb–Ta oxide mineral intergrowths (Table 7).

Wolframites within the albite granite are generally present as isolated subhedral to euhedral grains 5–60 μm in size that are occasionally intergrown with the columbite-group minerals (Fig. 5g–h). Concentrations of Nb_2O_5 + Ta_2O_5 (~3–10 wt%) are similar in all samples, but Mn# values (0.46 on average) are somewhat lower in the albite granites compared to wolframites in the alkali feldspar granites (Table 7, Fig. 6b).

4.3.5. Cassiterite

Within the alkali feldspar granites, cassiterite is present as homogeneous subhedral to euhedral crystals 2–20 μm in size that occur within the outer portions of the oxide mineral aggregates (Fig. 5a–d). Cassiterites within the albite granite are present rarely as subhedral to euhedral crystals ~100 μm in size that are intergrown with sulphides in the interstices between rock-forming minerals. Cassiterite in the granitic samples has broadly constant concentrations of Nb_2O_5 + Ta_2O_5 (on average 4.5 wt% for the MG alkali feldspar granite, 4.0 wt% for the FG alkali feldspar granite and 3.0 wt% for the albite granite) and FeO + MnO (on average 1.4 wt% for the MG alkali feldspar granite, 1.4 wt% for the FG alkali feldspar granite and 0.7 wt% for the albite granite) (Table 8). In a Nb + Ta vs. Fe + Mn diagram (Fig. 7), most grains plot between the 2:1 and 1:1 line, corresponding to the general substitution of columbite solid-solution in cassiterite: $3Sn^{4+} \Leftrightarrow 2(Nb, Ta)^{5+} + (Fe, Mn)^{2+}$ or $2Sn^{4+} \Leftrightarrow Fe^{3+} + (Nb, Ta)^{5+}$ (Černý and Ercit, 1989). It is noteworthy that cassiterite also occurs in skarn from the Laiziling pluton, although the skarn cassiterites are compositionally relatively pure with only trace amounts of Nb_2O_5 + Ta_2O_5 (0.07 wt% on average) and FeO + MnO (0.07 wt% on average).

4.4. Zircon

Zircons within the Laiziling granite are mostly present as euhedral prismatic crystals 5–40 μm wide that occur as inclusions within zinnwaldite and in interstices between the main rock-forming minerals (Fig. 8). The zircons are commonly homogeneous, lack obvious zoning and include some Th-rich uraninite and thorite. Occasionally zircon grains are surrounded by anhedral xenotime-(Y).

EPMA analyses indicate that zircons contain variable ZrO_2, HfO_2, ThO_2 and UO_2 concentrations (Table 9). Zircons within the MG alkali feldspar granite contain higher concentrations of ZrO_2 (61.7 wt% on average) than those within the FG alkali feldspar granite and albite granite (on average 59.8 and 59.4 wt%, respectively). The HfO_2 content is lowest (average of 2.0 wt%) in the MG alkali feldspar granite, increasing to 2.3 wt% (on average) in the FG alkali feldspar granite and

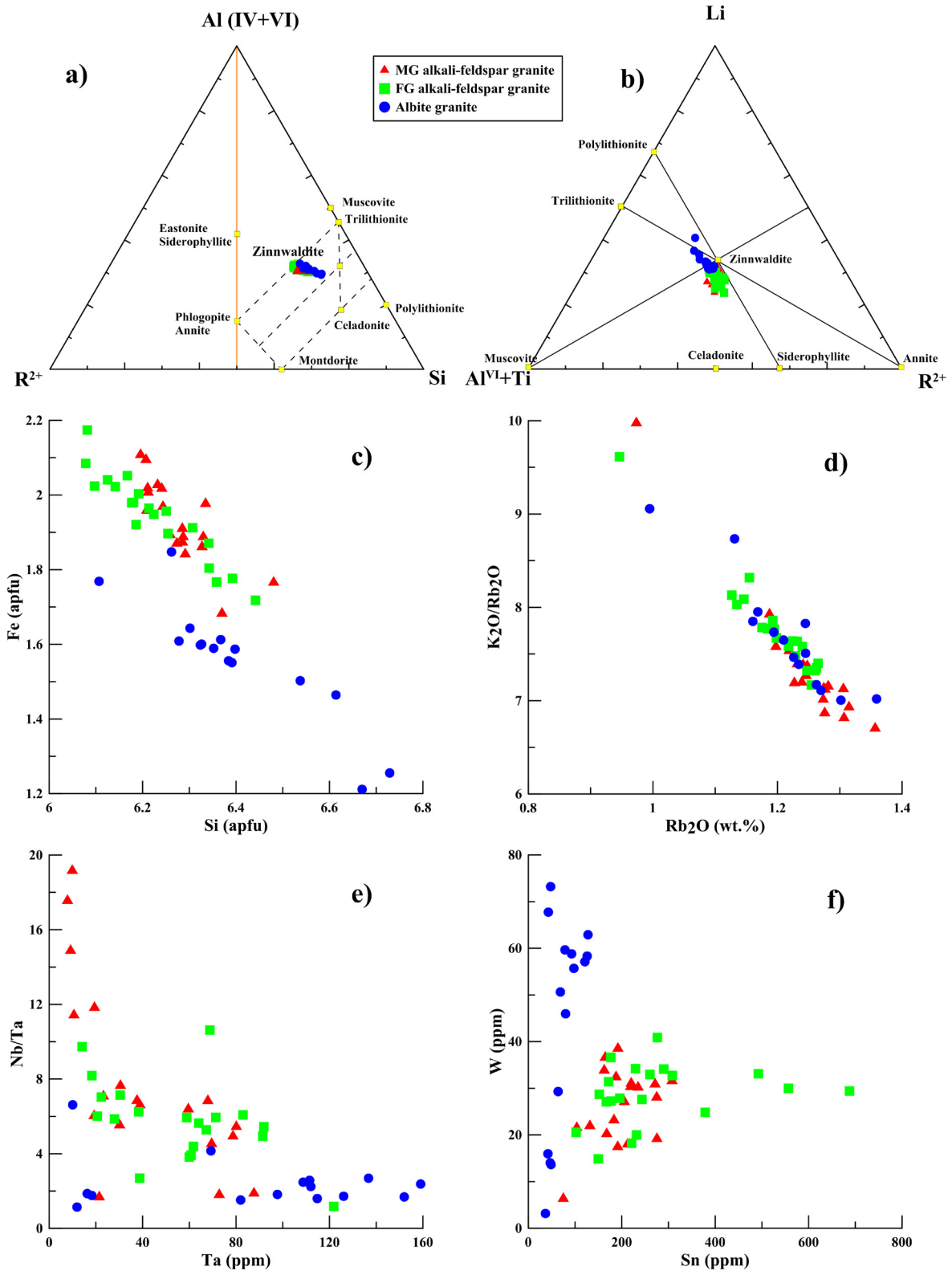

Fig. 4. (a) and (b) Classification and (c–f) major and trace element compositions of mica from the Laiziling granite. Modified after Rieder et al. (1996).

reaching 7.7 wt% (5.6 wt% on average) in the albite granite. Consequently, the average Zr/Hf ratios decrease and are 55.5, 45.3 and 19.5, respectively (Fig. 9a). Zircons within the albite granite have very low ThO_2 concentrations (average of 0.02 wt%), significantly lower than zircons within the alkali feldspar granites (average of 0.1 wt%) (Fig. 9b). There is no significant difference in the UO_2 content between samples.

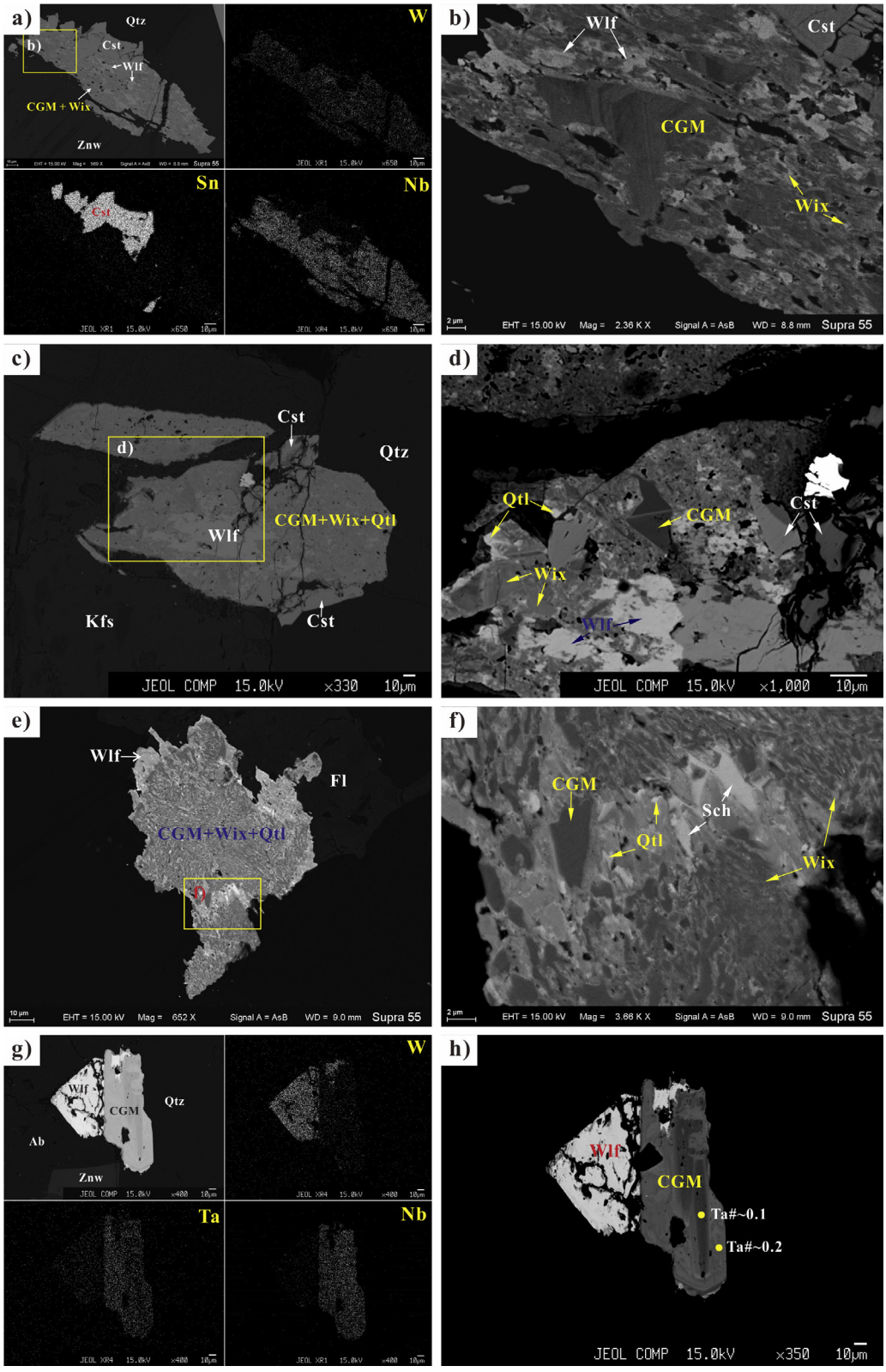

Fig. 5. BSE images and mappings showing the distribution of oxide minerals within the Laiziling granite. (a–b) Aggregate of columbite-group minerals, wolframoixiolite, wolframite and cassiterite in the MG alkali feldspar granite; (c–f) similar mineral aggregates in the FG alkali feldspar granite, also including qitianlingite, quartz and calcite; (g–h) columbite-group minerals intergrown with wolframite in the albite granite. Mineral abbreviations: columbite-group minerals (CGM); wolframoixiolite (Wix); qitianlingite (Qtl); wolframite (Wlf); cassiterite (Cst); scheelite (Sch).

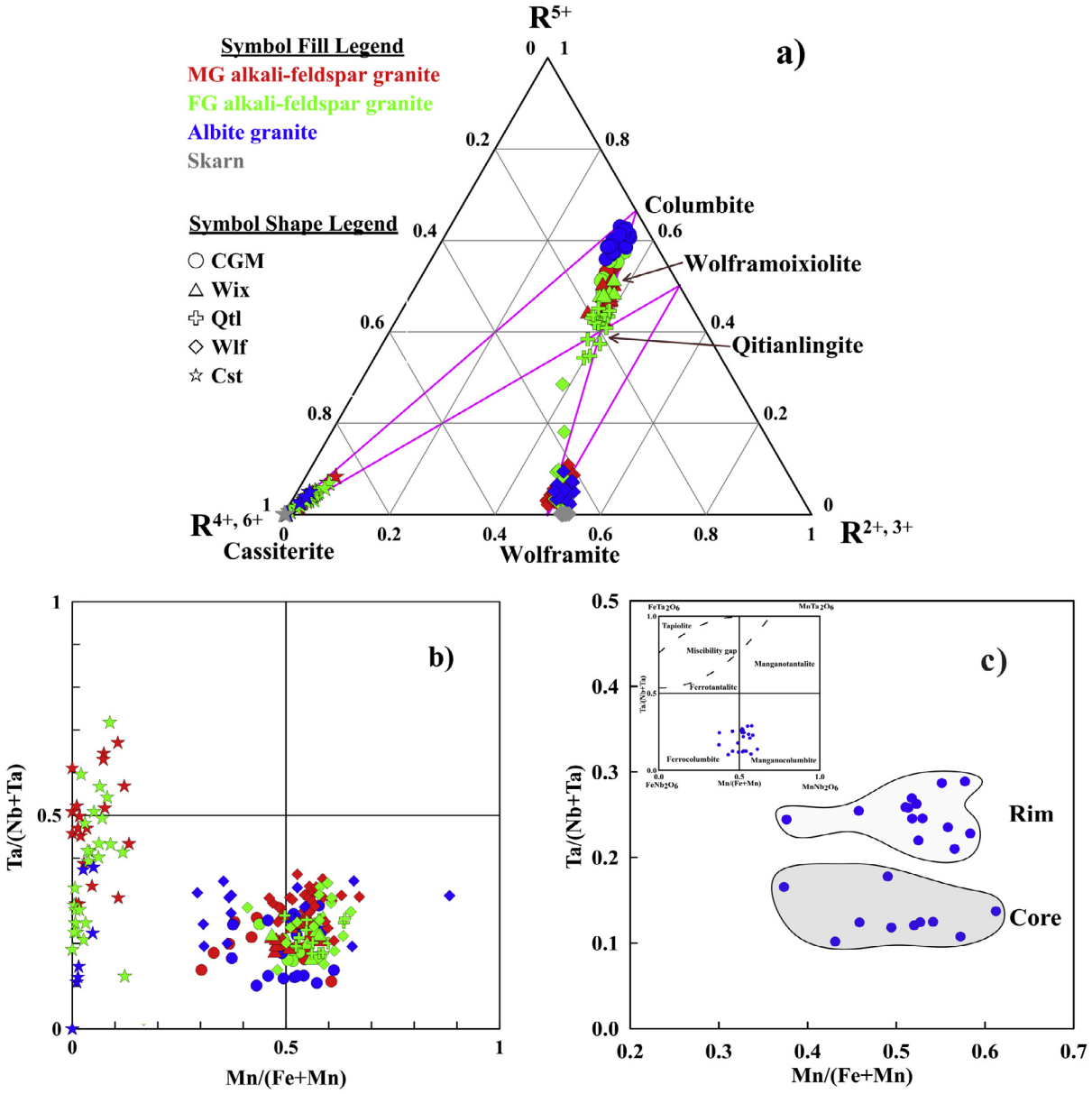

Fig. 6. (a) Ternary diagram showing the compositions and solid solution among the (Nb,Ta,W,Sn)-oxide minerals from the Laiziling granite and skarn; (b) compositional ranges and classification of oxide minerals from the Laiziling granite; (c) compositional variation of columbite-group minerals from the albite granite. The mineral abbreviations are as in Fig. 5.

5. Discussion

5.1. Fractionation patterns within the Laiziling pluton

Many minerals have been used as fractionation indicators for evolving granite systems and related pegmatites and aplites, such as Li-micas (Tischendorf et al., 1997), zircon and columbite-group minerals (Dostal and Chatterjee, 2000; Linnen, 1998; Linnen and Keppler, 2002; Novák et al., 2008; Breiter et al., 2017). During continuous differentiation of granitic plutons, the concentrations of Li, Rb and F in trioctahedral micas increase proportionally to their concentrations in the magma (Breiter et al., 2017), and the H_2O contents show an increasing trend from the early to late lithological zones with decreased solidus temperature (Li et al., 2017). The zinnwaldite in the Laiziling albite granite contains the highest Li_2O and F contents, which are up to 4.2 wt% (LA–ICP–MS), and 10.8 wt% (EMPA), respectively. These are much higher than equivalent concentrations (3.4 and 7.9 wt%, respectively) in micas from highly evolved analogues (ongonite and topazite) within the No. 431 dyke, located close to the Laiziling pluton (Huang et al., 2015). Commonly, the Rb and Cs contents of micas unequivocally indicate the most fractionated rare metal granite and pegmatite. The Rb_2O contents of the three granite phases fall in a similar range and reach values of 1.4 wt%, similar to concentrations in micas from highly evolved granites (e.g., 1.23 wt% in the Podlesí Stock, Breiter et al., 2017; 1.23 wt% in the Cínovec Pluton, Breiter et al., 2017). Furthermore, high Rb concentrations and reduced K/Rb ratios may be indicative of fractionation trends. The trioctahdedral and dioctahedral micas in the Yashan granite are characterized by < 5.2 wt % Rb_2O, which increases from the protolithionite granite to the lepidolite with decreasing K/Rb ratios (Li and Huang, 2013). However, the K/Rb ratio is constant in the zinnwaldite from the Laiziling granites. Our results suggest that the micas do not record fractional

Table 5
EMP compositions of columbite group minerals from the Laiziling granite.

	MG alkali-feldspar granite			FG alkali-feldspar granite			Albite granite			
	1	2	3	4	5	6	7	8	9	10
WO_3 (wt.%)	9.19	12.99	7.35	10.15	12.07	6.88	2.59	3.11	3.12	3.18
Nb_2O_5	50.63	43.62	53.99	46.14	45.11	54.42	58.93	60.73	47.29	48.12
Ta_2O_5	13.50	19.84	17.52	16.64	18.68	17.63	15.59	12.17	25.57	24.61
TiO_2	3.86	2.03	1.97	4.55	2.97	2.40	1.57	1.60	4.39	4.69
SnO_2	1.49	1.47	0.75	1.68	1.64	0.69	0.21	0.35	0.64	0.62
Sc_2O_3	0.28	0.15	0.15	0.29	0.23	0.23	0.12	0.10	0.73	0.74
MnO	6.05	8.16	10.51	6.58	7.12	9.96	12.59	11.76	9.08	9.81
FeO	14.17	11.44	8.95	13.47	12.42	9.45	8.08	8.90	8.56	7.86
Total	99.17	99.71	101.19	99.50	100.23	101.65	99.67	98.71	99.38	99.63
Calculated based on 6O										
W^{6+} (apfu)	0.146	0.215	0.116	0.163	0.196	0.107	0.041	0.049	0.050	0.051
Nb^{5+}	1.403	1.261	1.482	1.294	1.280	1.482	1.610	1.655	1.334	1.346
Ta^{5+}	0.225	0.345	0.289	0.281	0.319	0.289	0.256	0.199	0.434	0.414
Ti^{4+}	0.178	0.098	0.090	0.212	0.140	0.109	0.071	0.072	0.206	0.218
Sn^{4+}	0.036	0.037	0.018	0.041	0.041	0.017	0.005	0.008	0.016	0.015
Sc^{3+}	0.015	0.008	0.008	0.016	0.012	0.012	0.006	0.005	0.039	0.040
Mn^{2+}	0.314	0.442	0.540	0.346	0.378	0.508	0.644	0.601	0.480	0.514
Fe^{2+}	0.727	0.612	0.455	0.699	0.652	0.476	0.408	0.449	0.447	0.407
Sum	3.044	3.020	2.999	3.051	3.020	2.999	3.041	3.038	3.006	3.005
Mn/(Mn + Fe)	0.30	0.42	0.54	0.33	0.37	0.52	0.61	0.57	0.52	0.56
Ta/(Nb + Ta)	0.14	0.21	0.16	0.18	0.20	0.16	0.14	0.11	0.25	0.24

crystallization; nevertheless, a high degree of fractionation is supported by the higher Ta contents and lower Nb/Ta ratios of micas from the albite granite. The fractionation trend is also indicated by the increased Rb_2O concentration of the K-feldspars and the K_2O/Rb_2O ratios that decrease from the alkali feldspar to albite granite. These also indicate that the replacement of K by Rb in the minerals is not significant enough to indicate fractionation in the Laiziling granite.

The degree of fractionation inferred from zircon compositions is comparable to that deduced from micas. Zircon is the most common accessory mineral in metaluminous and peraluminous granites, and results in fractionation of Zr from Hf in the melt (Dostal and Chatterjee, 2000; Linnen and Keppler, 2002). Continuous compositional trends of zircon are evident in the rocks studied here, as detailed above, (i.e., with Hf concentrations and Zr/Hf ratios varying from 2.0 to 5.6 wt% and 55.5 to 19.5, respectively). The zircon saturation temperature (Watson and Harrison, 1983) of the Laiziling albite granite is ~700 °C, decreasing from ~760 °C in the MG alkali feldspar granite (Table 1).

Columbite-group minerals and other Nb–Ta oxide minerals (in particular wolframoixiolite and qintianlingite) only occur in more fractionated rare-element granite and granitic pegmatites (Novák et al., 2008; Alekseev et al., 2011; Dixon et al., 2014; Breiter et al., 2017). Cassiterites in the Laiziling granites show a solid solution towards the composition between $Fe^{3+}(Nb,Ta)O_4$ (the Fe-analogue of heftertjernite) and $(Fe,Mn)(Nb,Ta)_2O_6$ (columbite-group minerals). The observed trends are comparable to those in highly evolved granite and granitic pegmatite, along with multiple examples of mineralization related to rare-metal granitic plutons (Yin et al., 1995; Huang et al., 2002; Zhang et al., 2003; Breiter et al., 2007; Novák et al., 2008; Dixon et al., 2014).

The whole-rock compositions demonstrate that the Laiziling granites are metaluminous to peraluminous and most have high ACNK

Table 6
EMP compositions of wolframoixiolite and qitianlingite from the Laiziling granite.

	MG alkali-feldspar granite			FG alkali-feldspar granite					
	Wolframoixiolite			Wolframoixiolite			Qitianlingite		
	1	2	3	4	5	6	7	8	9
WO_3 (wt.%)	27.52	23.75	21.77	20.70	21.15	24.02	26.61	28.39	35.42
Nb_2O_5	32.42	34.57	38.34	37.29	38.23	37.82	36.99	31.57	29.65
Ta_2O_5	16.89	19.06	15.86	18.62	18.02	17.81	13.33	17.97	13.34
TiO_2	0.74	1.12	0.86	0.67	1.60	1.07	2.90	1.67	1.12
SnO_2	1.52	1.25	1.65	0.57	1.15	0.53	1.02	1.44	0.75
Sc_2O_3	0.20	0.24	0.18	0.19	0.21	0.17	0.31	0.14	0.21
MnO	10.74	11.44	10.56	11.71	11.60	11.59	11.84	11.10	10.59
FeO	10.30	9.16	10.66	8.92	8.51	8.58	8.45	9.24	9.49
Total	100.32	100.60	99.86	98.67	100.45	101.60	101.43	101.51	100.55
	Calculated based on 8O						Calculated based on 10O		
W^{6+} (apfu)	0.635	0.542	0.492	0.477	0.474	0.537	0.732	0.809	1.025
Nb^{5+}	1.306	1.376	1.512	1.499	1.496	1.474	1.775	1.570	1.497
Ta^{5+}	0.409	0.456	0.376	0.450	0.424	0.418	0.385	0.537	0.405
Ti^{4+}	0.050	0.074	0.056	0.045	0.104	0.069	0.231	0.138	0.094
Sn^{4+}	0.054	0.044	0.057	0.020	0.040	0.018	0.043	0.063	0.033
Sc^{3+}	0.015	0.019	0.014	0.015	0.016	0.013	0.028	0.013	0.021
Mn^{2+}	0.811	0.853	0.780	0.882	0.850	0.847	1.064	1.034	1.001
Fe^{2+}	0.767	0.675	0.778	0.663	0.616	0.619	0.750	0.849	0.886
Sum	4.046	4.039	4.064	4.051	4.020	3.995	5.008	5.014	4.961
Mn/(Mn + Fe)	0.51	0.56	0.50	0.57	0.58	0.58	0.59	0.55	0.53
Ta/(Nb + Ta)	0.24	0.25	0.20	0.23	0.22	0.22	0.18	0.26	0.21

Table 7
Compositions of wolframite from the Laiziling granite and skarn.

	MG alkali-feldspar granite			FG alkali-feldspar granite			Albite granite			Skarn	
	1	2	3	4	5	6	7	8	9	10	11
WO_3 (wt.%)	63.22	63.01	72.07	62.88	65.99	70.52	70.23	71.24	64.11	72.97	73.97
Nb_2O_5	6.13	5.82	2.25	6.99	5.36	1.84	1.73	2.03	4.39	0.11	0.11
Ta_2O_5	4.66	3.70	1.20	4.86	3.34	1.52	1.53	1.67	3.86	–	0.18
TiO_2	0.04	0.12	0.10	0.25	0.23	0.15	0.13	0.21	0.12	–	–
SnO_2	1.75	1.71	0.44	0.93	0.84	0.36	0.46	0.55	1.31	0.01	–
Sc_2O_3	0.24	0.29	0.20	0.27	0.25	0.15	0.13	0.19	0.29	–	0.03
MnO	12.99	13.45	13.23	10.97	13.39	14.21	16.80	12.43	8.67	7.57	15.87
FeO	11.04	11.48	10.18	12.59	10.88	10.46	8.80	11.31	16.04	18.35	9.20
Total	100.07	99.58	99.65	99.74	100.27	99.20	99.81	99.63	98.79	99.02	99.37
Calculated based on 4O											
W^{6+} (apfu)	0.807	0.806	0.935	0.801	0.840	0.920	0.911	0.925	0.833	0.962	0.971
Nb^{5+}	0.136	0.130	0.051	0.155	0.119	0.042	0.039	0.046	0.100	0.003	0.002
Ta^{5+}	0.062	0.050	0.016	0.065	0.045	0.021	0.021	0.023	0.053		0.002
Ti^{4+}	0.002	0.004	0.004	0.009	0.008	0.006	0.005	0.008	0.005		
Sn^{4+}	0.034	0.034	0.009	0.018	0.016	0.007	0.009	0.011	0.026	0.000	
Sc^{3+}	0.010	0.013	0.009	0.012	0.011	0.007	0.006	0.008	0.013		0.002
Mn^{2+}	0.542	0.563	0.561	0.457	0.557	0.606	0.712	0.528	0.368	0.326	0.681
Fe^{2+}	0.454	0.474	0.426	0.517	0.447	0.440	0.368	0.474	0.672	0.781	0.390
Sum	2.048	2.074	2.011	2.035	2.044	2.049	2.071	2.023	2.069	2.072	2.049
$Nb^{5+} + Ta^{5+}$	0.199	0.180	0.067	0.220	0.164	0.063	0.060	0.069	0.152	0.003	0.005
Mn/(Mn + Fe)	0.54	0.54	0.57	0.47	0.55	0.58	0.66	0.53	0.35	0.29	0.64
Ta/(Nb + Ta)	0.31	0.28	0.24	0.29	0.27	0.33	0.35	0.33	0.35	0.00	0.50

Table 8
Representative compositions of cassiterite from the Laiziling granite and skarn.

	MG alkali-feldspar granite			FG alkali-feldspar granite			Albite granite			Skarn		
	1	2	3	4	5	6	7	8	9	10	11	12
WO_3 (wt.%)	–	0.06	0.04	0.62	0.27	0.57	–	0.16	0.52	–	0.13	0.05
Nb_2O_5	2.16	1.76	1.79	2.31	1.62	3.09	2.18	1.95	3.04	0.02	–	–
Ta_2O_5	2.96	1.21	2.94	3.56	1.10	1.50	2.21	0.55	0.69	0.04	–	–
TiO_2	0.25	0.51	0.84	0.24	0.39	0.67	1.27	0.08	0.15	0.06	0.11	0.04
SnO_2	92.27	95.68	92.19	91.11	95.30	92.06	92.68	96.42	94.64	99.52	99.76	99.96
Sc_2O_3	–	–	–	–	–	–	–	–	–	–	–	–
MnO	0.03	0.01	0.03	0.05	0.00	0.01	0.06	0.01	0.01	–	0.03	–
FeO	1.54	1.04	1.50	1.55	0.94	1.77	1.08	0.80	1.06	0.01	0.01	0.13
Total	99.21	100.27	99.31	99.44	99.62	99.68	99.48	99.97	100.13	99.64	100.04	100.17
Calculated based on 2O												
W^{6+} (apfu)		0.000	0.000	0.004	0.002	0.004		0.001	0.003		0.001	0.000
Nb^{5+}	0.025	0.020	0.020	0.026	0.018	0.035	0.024	0.022	0.034	0.000		
Ta^{5+}	0.020	0.008	0.020	0.024	0.007	0.010	0.015	0.004	0.005	0.000		
Ti^{4+}	0.005	0.009	0.016	0.005	0.007	0.012	0.024	0.002	0.003	0.001	0.002	0.001
Sn^{4+}	0.923	0.944	0.918	0.910	0.948	0.908	0.915	0.956	0.933	0.998	0.996	0.997
Sc^{3+}												
Mn^{2+}	0.001	0.000	0.001	0.001	0.000	0.000	0.001	0.000	0.000		0.001	
Fe^{2+}	0.032	0.022	0.031	0.032	0.020	0.037	0.022	0.017	0.022	0.000	0.000	0.003
Sum	1.005	1.004	1.006	1.002	1.002	1.005	1.002	1.002	1.000	1.000	1.000	1.001
$Nb^{5+} + Ta^{5+}$	0.045	0.028	0.040	0.050	0.026	0.045	0.039	0.026	0.039	0.000	0.000	0.000
$Fe^{2+} + Mn^{2+}$	0.033	0.022	0.032	0.033	0.020	0.037	0.024	0.017	0.022	0.000	0.001	0.003

(1.1–2) values. The zoned Laiziling pluton varies from alkali feldspar granite at the bottom to albite granite at the top, along with an elemental increasing of Na2O and F and decreasing of CaO and Sr, indicative of magmatic evolution. This is in contrast with the F-rich albitization zone, which is characterized by increased, or unchanged, CaO and Sr concentrations (Schwartz, 1992). The concentrations of high-field-strength elements (HFSEs) (total REE, Zr, Th and Y) decrease progressively, and concentrations of the alkali metals and ore elements (Li, Rb, Nb, Ta and W) increase significantly. Some whole-rock compositional parameters are indicative of fractionation, including the progressive decrease in Zr/Hf, Nb/Ta and Th/U ratios, together with the near-identical chondrite-normalized REE patterns and negative Eu anomalies (Bau, 1997; Linnen and Keppler, 1997, 2002).

Therefore, the mineralogical and geochemical signatures of the Laiziling granites indicate that the rocks are highly evolved and record the magmatic differentiation with a progressive fractionation of plagioclase from the base to the roof of the pluton.

5.2. W–Nb–Ta mineralization in the alkali feldspar granite: Magmatic or hydrothermal?

In the Laiziling alkali feldspar granite, W is concentrated in the W–Nb–Ta oxide minerals, including disseminated wolframite, qitianlingite, wolframoixiolite and columbite-group minerals. Understanding the genesis of this W-rich mineral assemblage is important to better understand the polymetal mineralization in the granite.

5.2.1. Fluorine enrichment and the formation of columbite-group minerals

The Laiziling granite contains fluorine, with topaz as the main F-

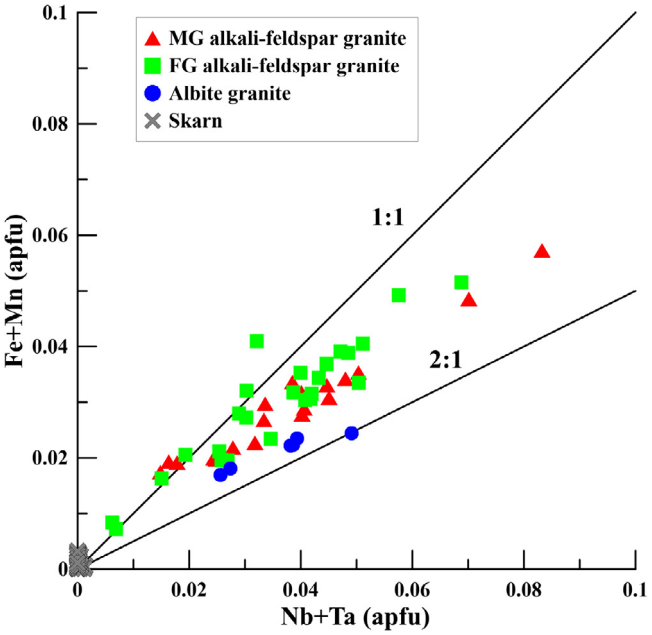

Fig. 7. Plots of cassiterite compositions in the Laiziling granite and skarn.

enriched mineral. The stability of topaz in natural felsic systems is related to the peraluminosity of the system, and calcia and silica activity, and is linked to rock-forming mineral buffers by corresponding chemical potentials (Dolejš and Baker, 2004). The crystallization of topaz is restricted to peraluminous conditions, which is consistent with the presence of Li-micas or anhydrous aluminosilicates. Under near-solidus conditions, quartz, K-feldspar, plagioclase, and topaz are the stable mineral assemblage, thus representing Ca-bearing topaz granites. F-topaz end number becomes unstable with decreasing temperature (Barton, 1982), causing enrichment of the topaz solid solution in the hydroxyl end-member (Dolejš and Baker, 2004). The topaz is suggested to have a magmatic origin based on it being intergrown with the other main rock-forming minerals, and because F is enriched in the primary Laiziling granitic melts.

The columbite-group minerals that exhibit oscillatory zoning are potentially magmatic products (Fig .5b), as Nb and Ta preferentially partition into melt (Timofeev and Williams-Jones, 2015; Timofeev et al., 2017). The experimental study by Borodulin et al. (2009) indicated that in aqueous F-bearing fluid, water-saturated Li- and F-rich haplogranite melts at temperatures of 650 °C–750 °C and a pressure of 100 MPa, and the partition coefficients of Ta and Nb between the fluid and the granitic melt are extremely low (weight ratio $^{\text{fluid/melt}}D_{\text{Ta}}$ = 0.001–0.008 and $^{\text{fluid/melt}}D_{\text{Nb}}$ = 0.001–0.022, respectively). The above section shows that the Laiziling granites are the products of fractional crystallization of a Li–F-rich granitic magma. High fluorine concentrations could lower the solidus temperature and prolong the

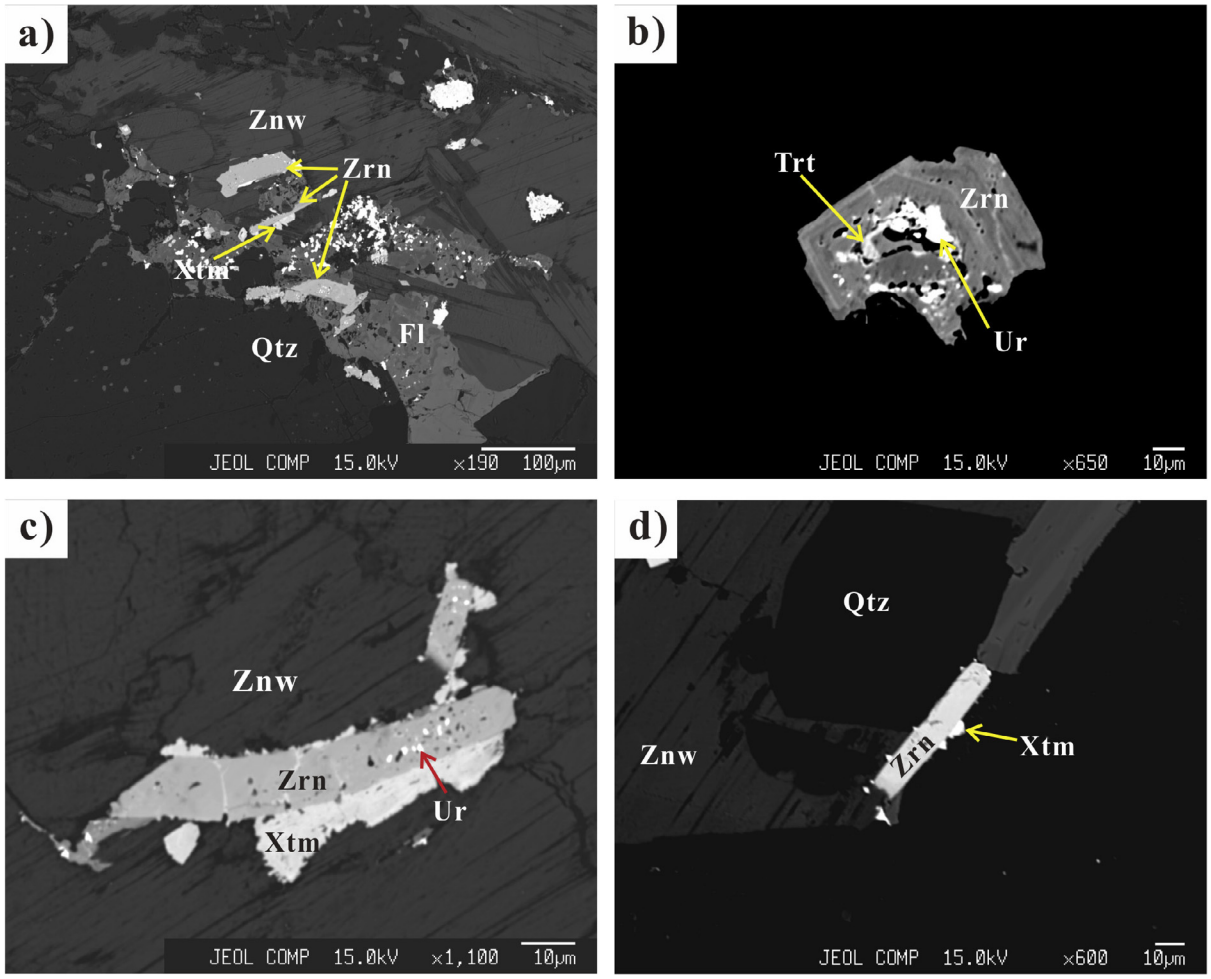

Fig. 8. BSE images of zircon from the Laiziling granite. (a–b) Zircons in the MG alkali feldspar granite; (c) zircon intergrown with xenotime within the FG alkali feldspar granite; (d) euhedral homogeneous zircon from the albite granite. Mineral abbreviations: Zrn – zircon; Xtm – xenotime; Fl – fluorite; Trt – thorite; Ur – uraninite.

Table 9
Chemical compositions of zircons from the Laiziling granite.

	MG alkali-feldspar granite				FG alkali-feldspar granite				Albite granite			
	1	2	3	4	5	6	7	8	9	10	11	12
P_2O_5 (wt.%)	0.21	0.41	–	0.45	0.03	0.05	0.23	0.37	0.02	0.04	0.01	–
SiO_2	33.48	32.64	32.70	32.76	31.87	33.30	32.05	32.40	32.93	33.01	32.62	32.73
ZrO_2	62.24	62.90	64.72	62.97	59.66	62.79	60.41	62.40	58.81	61.51	59.95	60.11
HfO_2	2.13	1.39	1.30	1.92	3.21	2.67	2.35	1.83	6.85	4.57	5.12	5.89
ThO_2	0.01	0.09	0.03	0.05	0.01	0.03	0.12	0.03	0.01	0.02	–	–
UO_2	0.77	1.58	0.20	1.38	1.90	0.77	1.94	1.79	0.93	1.37	1.03	1.00
Al_2O_3	0.15	0.14	–	0.08	0.31	–	–	–	0.12	–	0.13	0.03
Y_2O_3	0.34	0.46	0.11	0.53	0.32	0.08	0.47	0.48	0.09	0.08	0.27	0.08
CaO	0.05	0.02	0.03	0.05	0.40	0.06	0.36	0.22	0.09	0.10	0.18	0.11
FeO	0.36	0.01	0.35	0.58	0.53	0.05	0.67	0.63	0.15	–	0.13	0.12
PbO	–	0.02	–	–	–	0.02	–	0.05	–	–	–	–
Total	99.75	99.67	99.43	100.77	98.24	99.82	98.60	100.21	99.98	100.68	99.45	100.08
P (apfu)	0.006	0.011		0.012	0.001	0.001	0.006	0.010	0.000	0.001	0.000	
Si	1.026	1.007	1.008	1.002	1.009	1.025	1.009	1.001	1.028	1.020	1.020	1.021
Zr	0.930	0.946	0.973	0.940	0.921	0.942	0.927	0.940	0.896	0.927	0.914	0.914
Hf	0.019	0.012	0.011	0.017	0.029	0.023	0.021	0.016	0.061	0.040	0.046	0.052
Th	0.000	0.001	0.000	0.000	0.000	0.000	0.001	0.000	0.000	0.000		
U	0.005	0.011	0.001	0.009	0.013	0.005	0.014	0.012	0.006	0.009	0.007	0.007
Al	0.005	0.005		0.003	0.012				0.004		0.005	0.001
Y	0.002	0.001	0.001	0.002	0.014	0.002	0.012	0.007	0.003	0.003	0.006	0.004
Ca	0.002	0.001	0.001	0.002	0.014	0.002	0.012	0.007	0.003	0.003	0.006	0.004
Fe	0.009	0.000	0.009	0.015	0.014	0.001	0.018	0.016	0.004		0.004	0.003
Pb		0.000				0.000		0.000				
Zr/Hf	49.84	77.19	85.24	56.17	31.80	40.12	43.91	58.15	14.68	23.01	20.02	17.43

crystallization time (Manning, 1981), thereby increasing the concentrations of Nb and Ta. Despite the albite granite having high Li and F concentrations, no relationship is found between the abundance of Nb–Ta oxide minerals and the F concentration. This may be due to fluorine being less important than previously thought in terms of controlling the behaviours of Nb and Ta in highly evolved granitic melts relative to melt compositions (ASI, molarAl/[Na + K + Li], Fiege et al., 2011; Aseri et al., 2015). In addition, the absence of tantalite in the Laiziling granite may be due to the low Ta concentration and higher tantalite-(Mn) solubility than columbite-(Mn) in the granitic melts, which increases with increasing temperature and Li content of the melt (Linnen, 1998; Aseri et al., 2015).

Fluorine enrichment increases zircon solubility, in contrast to the constant Nb–Ta solubility in the F-bearing melt (Aseriet al., 2015). The whole-rock Zr concentration decreases from 100 ppm in the alkali-feldspar granite to 40 ppm in the albite granite, while Nb and Ta increase in the Laiziling pluton. This could explain the low zircon saturation temperature and the trend of decreasing whole-rock Zr contents from alkali feldspar granite to albite granite.

5.2.2. W Mineralization indicated by the occurrence of W–Nb–Ta oxide aggregates

In the Laiziling granitic melt, with the exception of the columbite-group minerals, the other W-enriched Nb–Ta minerals (wolframoixiolite and qitianlingite) began to precipitate around the columbite-group minerals. The columbite-group minerals show limited solid solution towards wolframite (WO_3 content ranging from 5 to 15 wt%), suggesting W was concentrated in the original melt. Wolframoixiolite and qitianlingite lie on a solid solution trend between columbite and wolframite, and are characterized by large variations in W but moderate and near constant Mn/(Mn + Fe) and Ta/(Ta + Nb) ratios, recording solid solution towards wolframite. The wolframite is rich in Nb and Ta (Nb_2O_5 + Ta_2O_5 contents of 2–12 wt%) compared with hydrothermal wolframite within the Laiziling skarn (< 0.3 wt% Nb_2O_5 + Ta_2O_5). It may be concluded that the crystal structures of W–Nb–Ta oxide minerals restricts the substitution of Nb–Ta for W, and crystallized variable oxide minerals by ordering the cations along the layers formed by octahedron chains (Voloshin, 1993). Therefore, it is implied that the granite-hosted W mineralization formed at the same time as the Nb–Ta mineralization in the Laiziling alkali feldspar granite, due to the formation of the complex W–Nb–Ta oxide mineral aggregates.

5.2.3. Fluid-rich magma for W–Nb–Ta mineralization

The occurrences of qitianlingite and wolframoixiolite as isolated grains or together with wolframite are known elsewhere, and sometimes termed W-rich columbite or Nb-wolframite (Johan and Johan, 1994). Most occurrences of these minerals are interpreted to be the products of late-stage fluid enrichment in magmatic systems, including examples that are disseminated within the transition zone between zinnwaldite granite and protolithionite granite (Johan and Johan, 1994), topaz–zinnwaldite granite (Ginzburg et al., 1969; Margnac et al., 2001; Alekseev et al., 2011), biotite granite (Breiter et al., 2017), pegmatite (Peng et al., 1988; Novák et al., 2008) and ongonite (albite granite analogue; Huang et al., 2015). Also, qitianlingite and wolframoixiolite may form at comparatively lower temperatures during the early hydrothermal stages within W-enriched quartz veins (Zhang et al., 2003), greisen (Breiter et al., 2017), W-rich granitic porphyry (Ding et al., 2017) and as exsolution of Nb-rutile in pegmatite (Černý and Chapman, 2001; Černý et al., 2007). The qitianlingite and wolframoixiolite in the Laiziling granite occur around zoned columbite-group minerals within the complex W–Nb–Ta oxide mineral aggregates. The columbite-group minerals present in the center of the mineral aggregates commonly have irregular margins and are apparently replaced by W-rich oxide mineral aggregates, indicating the breakdown of columbite-group minerals grains and possible late magmatic metasomatism (Wu et al., 2017). The occurrence of W-enriched oxide mineral aggregates in the Laiziling alkali feldspar granite was most likely the product of reaction between the columbite-group minerals and later W-enriched fluids during the post-magmatic stage, when the last pockets of highly fractionated melt and aqueous fluids formed. The protons (H^+) and H_2O enriched in these fluids should promote strongly the formation of wolframite though reaction of an acidic, metal-bearing fluid with muscovite (Wood and Samson, 2000; Wu et al., 2017). Otherwise, the presence of carbonate is consistent with calcite that is occasionally present in the W-rich oxide mineral aggregates within the Laziling alkali feldspar granite. It is possibly that minor HCO_3^- and CO_2

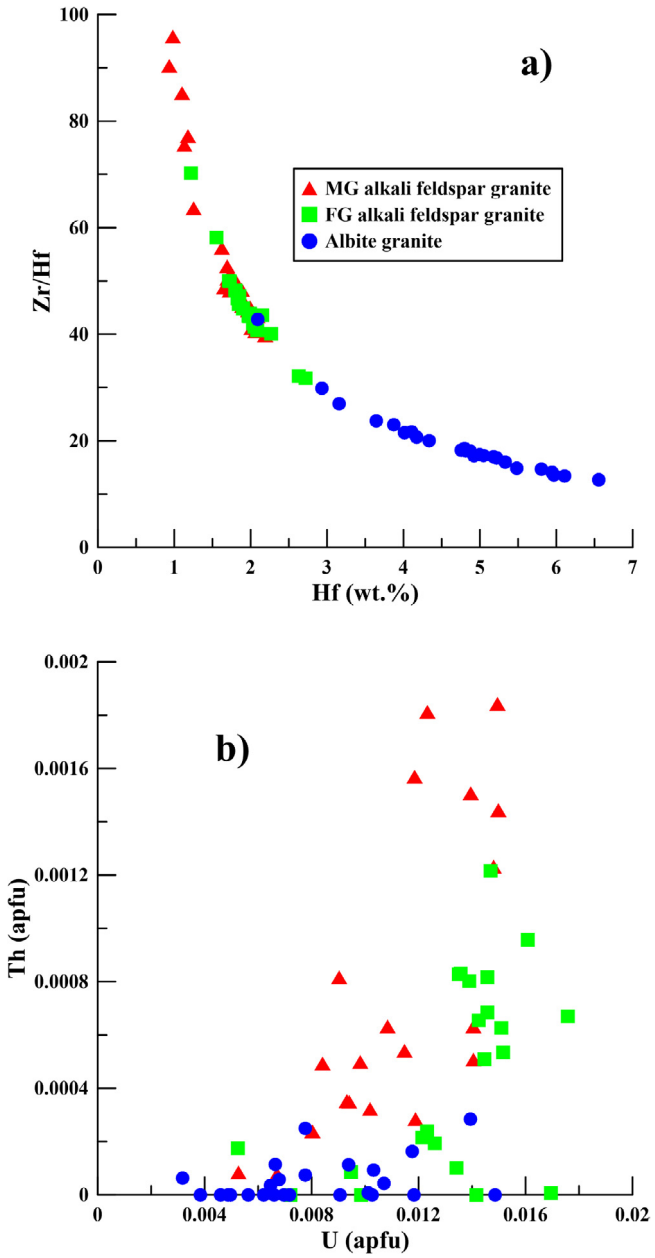

Fig. 9. Zr/Hf variations in zircon from the Laiziling granite.

should occur in the fluid may be responsible for W transport (Higgins, 1980). In addition, the patchy and "symplektitic-like" texture of the aggregates supports this hypothesis. The small variations in Ta# and Mn# values observed in the variably W-enriched oxide minerals also suggest a very low mobility of these elements during subsolidus reactions (Novák and Černý, 1998).

5.3. W–Sn mineralization in the Laiziling albite granite: Intensive fluid activity

The intergrowths of columbite-group minerals and wolframite in the Laiziling albite granite have close to end-member compositions. That is, the columbite-group minerals contain less W and the wolframite contains less Nb and Ta than those present in the alkali feldspar granites, and wolframoixiolite and qitianlingite are absent. Tungsten commonly behaves as an incompatible element in peraluminous granitic melts (Raimbault and Azencott, 1987) and wolframite could not easily attain saturation (Linnen and Cuney, 2005; Che et al., 2013). However, columbite in the albite granite is obviously zoned in which the outer part has elevated Ta#, which is characteristic of magmatic fractionation. Thus, the petrogenesis of this mineral assemblage, and whether or not it required a subsequent hydrothermal event, is unclear. The whole-rock Nb/Ta ratios in the Laiziling albite granite decrease sharply to 2 from 5 in the Laiziling alkali feldspar granites. Ballouard et al. (2016) concluded that Nb/Ta $<$ 5 in peraluminous granites indicate alteration during the transition from the magmatic to hydrothermal stage. We infer that the Laiziling albite granite went through a similar hydrothermal stage. Also we note that the core of zoned columbite is altered and has embayed boundaries, and was subsequently overgrown by a Ta-rich rim. A few studies have suggested that Nb–Ta may locally be remobilized during hydrothermal alteration (Zaraisky et al., 2010), in which the later fluids overprinting the magmatic system are characteristic of the network-type morphology of tantalite (Rao et al., 2009) and the patchy Ta-rich columbite-group minerals that overgrow the primary Nb–Ta minerals (Zhu et al., 2015). Therefore, we suggest that increased fluid activity may have enhanced co-precipitation and intergrowth of wolframite and columbite, and that the deficiency of wolframoixiolite and qitianlingite in the Laiziling albite granite is consistent with high concentrations of volatiles (in particular 3 wt% F and H_2O) and Li (2600 ppm). The decrease in the W content of the latest crystallized columbite-group minerals in the Laiziling albite granite may be related to a fluid phases that rapidly exsolved from the magma leading to strong fractionation of W into the melt (Belkasmi et al., 2000) in which increased W is partitioned into the lattice of the micas and wolframite.

Fluid enrichment in the peraluminous melt should also trigger hydrothermal processes appropriate for Sn mineralization. The whole-rock Sn concentration in the Laiziling granite is only ~20 ppm, far lower than the solubility of cassiterite in melt close to an oxygen fugacity at the NNO (Ni-NiO) buffer at 700 °C (0.32 wt%; Bhalla et al., 2005). The cassiterite in the Laiziling granite overgrows the W–Nb–Ta mineral aggregates and formed within the interstices between the rock-forming minerals, and contains Nb_2O_5 + Ta_2O_5 contents (2–6 wt%) that are significantly different from cassiterite crystals formed at low temperature (Tindle and Breaks, 1998). The cassiterite intergrown with sulphide in the Laiziling skarn, which also hosts wolframite and Sn-bearing titanite, is deficient in Nb and Ta. The tiny cassiterite grains within the albite granite possibly grew from percolating subsolidus fluids upon cooling.

6. Conclusions

The Laiziling granitic complex included three intrusive phases, from base upward, consists of a medium-grained alkali feldspar granite, fine-grained alkali feldspar granite and albite granite. Micas from three phases all belong to the zinnwaldite group. Based on whole-rock geochemical and mineralogical characteristics, granites from Laiziling are highly evolved and developed along a progressive fractionation trend. Oxide mineral aggregates of columbite-group minerals, wolframoixiolite, qitianlingite, wolframite and cassiterite record a prolonged event of W–Nb–Ta mineralization from the magmatic to hydrothermal stages. The high degrees of magmatic fractionation largely controlled the Nb–Ta mineralization; magmatic columbite-(Fe)–columbite-(Mn), present as oscillatory zoned crystals, crystallized in the highly evolved W–Nb–Ta-rich melt. At the magmatic–hydrothermal transition, fluids rich in W results in the breakdown and alteration of columbite and formation of the W–Nb–Ta oxide mineral aggregates, which include wolframoixiolite, qitianlingite, wolframite ± scheelite, quartz and calcite. Subsequently enhanced fluid activity during the hydrothermal stage resulted in the final W–Sn phase of mineralization in the Laiziling granite. Disseminated wolframite and cassiterite in the granite are Nb–Ta rich, clearly different from those of skarns from the Laiziling district.

Acknowledgements

This study was financially supported by the National Natural Science Foundation of China (Grant Nos. 41572045 and 41230315), the National Key R & D Program of China (Grant No. 2016YFC0600203), and the Caiyuanpei program from China Scholarship Council (CSC). Comments from two anonymous reviewers greatly improved the manuscript.

References

Alekseev, V.I., Gembitskaya, I.M., Marin, Y.B., 2011. Wolframoixiolite and niobian ferberite from zinnwaldite granitic rocks of the Chukchi Peninsula. Geol. Ore Deposits 53 (7), 639–648.
Aseri, A.A., Linnen, R.L., Che, X.D., Thibault, Y., Holtz, F., 2015. Effects of fluorine on the solubilities of Nb, Ta, Zr and Hf minerals in highly fluxed water-saturated haplogranitic melts. Ore Geol. Rev. 64, 736–746.
Badanina, E.V., Sitnikova, M.A., Gordienko, V.V., Melcher, F., Gäbler, H.E., Lodziak, J., Syritso, L.F., 2015. Mineral chemistry of columbite–tantalite from spodumene pegmatites of kolmozero, kola peninsula (russia). Ore Geol. Rev. 64 (1), 720–735.
Bau, M., 1997. The lanthanide tetrad effect in highly evolved felsic igneous rocks – a reply to the comment by Y Pan. Contrib. Mineral. Petrol. 128 (4), 409–412.
Ballouard, C., Poujol, M., Boulvais, P., Branquet, Y., Tartèse, R., Vigneresse, J., 2016. Nb-Ta fractionation in peraluminous granites: a marker of the magmatic-hydrothermal transition. Geology 44, 231–234.
Barton, M.D., 1982. The thermodynamic properties of topaz solid solutions and some petrologic applications. Am. Mineral. 67, 956–974.
Belkasmi, M., Cuney, M., Pollard, P.J., Bastoul, A., 2000. Chemistry of the ta-nb-sn-w oxide minerals from the yichun rare metal granite (SE china): genetic implications and comparison with moroccan and french hercynian examples. Mineral. Mag. 64 (3), 507–523.
Bhalla, P., Holtz, F., Linnen, R.L., Behrens, H., 2005. Solubility of cassiterite in evolved granitic melts: effect of T, fO_2, and additional volatiles. Lithos 80 (1–4), 387–400.
Borodulin, G.P., Chevychelov, V.Y., Zaraysky, G.P., 2009. Experimental study of partitioning of tantalum, niobium, manganese, and fluorine between aqueous fluoride fluid and granitic and alkaline melts. Doklady Earth Sci. 427 (1), 868–873.
Breiter, K., Lamarão, C.N., Borges, R.M.K., Dall'Agnol, R.D., 2014. Chemical characteristics of zircon from A-type granites and comparison to zircon of S-type granites. Lithos 192–195, 208–225.
Breiter, K., Škoda, R., Uher, P., 2007. Nb–Ta–Ti–W–Sn-oxide minerals as indicators of a peraluminous P-and F-rich granitic system evolution: Podlesí, Czech Republic. Mineral. Petrol. 91, 225–248.
Breiter, K., Vaňková, M., Galiová, M.V., Korbelová, Z., Kanický, V., 2017. Lithium and trace-element concentrations in triotahedral micas from granites of different geochemical types measured via laser ablation ICP-MS. Mineral. Mag. 81 (1), 15–33.
Černý, P., Chapman, R., 2001. Exsolution and breakdown of scandian and tungstenian Nb–Ta–Ti–Fe–Mn phases in niobian rutile. Can. Mineral. 39 (1), 93–101.
Černý, P., Ercit, T.S., 1989. Mineralogy of niobium and tantalum: crystal chemical relationships, paragenetic aspects and their economic implications. In: Möller, P., Černý, P., Saupé, F. (Eds.), Lanthanides, Tantalum and Niobium. Special Publication No. 7 of the Society for Geology Applied to Mineral Deposits, pp. 27–79.
Černý, P., Goad, B.E., Hawthorne, F.C., Chapman, R., 1986. Fractionation trends of the nb- and ta-bearing oxide minerals in the greer lake pegmatitic granite and its pegmatite aureole, southeastern manitoba. Am. Mineral. 71 (3), 501–517.
Černý, P., Novák, M., Chapman, R., Ferreira, K., 2007. Subsolidus behavior of niobian rutile from the Písek region, Czech Republic: a model for exsolution in W-and $Fe^{2+} > > Fe^{3+}$-rich phases. J. Geosci. 52, 143–159.
Che, X.D., Linnen, R.L., Wang, R.C., Aseri, A., Thibault, Y., 2013. Tungsten solubility in evolved granitic melts: an evaluation of magmatic wolframite. Geochimica Et Cosmochimica Acta 106 (4), 84–98.
Cuney, M., Marignac, C., Weisbrod, A., 1992. The beauvoir topaz-lepidolite albite granite (massif central, france); the disseminated magmatic Sn-Li-Ta-Nb-Be mineralization. Econ. Geol. 87 (7), 1766–1794.
Ding, T., Ma, D.S., Lu, J., Zhang, R.Q., Zhang, S.T., 2017. Mineral geochemistry of granite porphyry in Huangshaping polymetalic deposit, southern Hunan Province, and its implications for metalogensis of skarn scheelite mineralization. Acta Petrologica Sinica 3 (3), 716–728 (in Chinese with English abstract).
Dixon, A., Cempírek, J., Groat, L.A., 2014. Mineralogy and geochemistry of pegmatites on Mount Begbie, British Columbia. Can. Mineral. 52, 129–164.
Dolejš, D., Baker, D.R., 2004. Thermodynamic analysis of the system Na_2O-K_2O-CaO-Al_2O_3-SiO_2-H_2O-F_2O_{-1}: Stability of fluorine-bearing minerals in felsic igneous suites. Contrib. Mineral. Petrol. 146, 762–778.
Dostal, J., Chatterjee, A.K., 2000. Contrasting behaviour of nb/ta and Zr/Hf ratios in a peraluminous granitic pluton (Nova Scotia, Canada). Chem. Geol. 163 (1), 207–218.
Fiege, A., Kirchner, C., Holtz, F., Linnen, R.L., Dziony, W., 2011. Influence of fluorine on the solubility of manganotantalite ($MnTa_2O_6$) and manganocolumbite ($MnNb_2O_6$) in granitic melts- an experimental study. Lithos 122, 165–174.
Galliski, M.A., Marquez-Zavalia, M.F., Cerny, P., Martinez, V.A., Chapman, R., 2008. The Ta-Nb-Sn-Ti oxide-mineral paragenesis from La Viquita, a spodumene-bearing rare-element granitic pegmatite, San Luis, Argentina. Can. Mineral. 46 (2), 379–393.
Gao, J.F., Zhou, M.F., Lightfoot, P.C., Wang, C.Y., Qi, L., Sun, M., 2013. Sulfide saturation and magma emplacement in the formation of the Permian Huangshandong Ni–Cu sulfide deposit, Xinjiang, Northwestern China. Econ. Geol. 108, 1833–1848.
Ginzburg, A.I., Gorzhevskaya, S.A., Sidorenko, G.A., 1969. Wolframoixiolite—a Variety of Ixiolite. Zap. Vses. Miner. O-va 98 (1), 63–73.
Higgins, N.C., 1980. Fluids inclusion evidence for transport of tungsten by carbonate complexes in hydrothermal solutions. Can. J. Earth Sci. 17 (7), 823–830.
Hu, M.Y., Fan, X.T., Stoll, B., Kuzmin, D., Liu, Y.S., Liu, Y., Sun, W.D., Wang, G., Zhan, X.C., Jochum, K.P., 2011. Preliminary characterisation of new reference materials for microanalysis: Chinese geological standard glasses CGSG-1, CGSG-2, CGSG-4 and CGSG-5. Geostandards Geoanal. Res. 35 (2), 235–251.
Hu, Y.J., H, X.G., Zheng, R.F., 1982. Thematic report on Pb-Zn polymetallic metallogenic regulation and ore-prospecting of South Hunan. Hunan Institute of Geology Changsha, China (in Chinese with English abstract).
Hua, R.M., Mao, J.W., 1999. A preliminary discussion on the Mesozoic metallogenic explosion in East China. Miner. Deposits 18, 300–308 (in Chinese with English abstract).
Hua, R.M., Chen, P.R., Zhang, W.L., Liu, X.D., Lu, J.J., Lin, J.F., Yao, J.M., Qi, H.W., Zhang, Z.S., Gu, S.Y., 2003. Metallogenic systems related to Mesozoic and Cenozoic granitoids in South China. Sci. China Ser. D: Earth Sci. 46 (8), 816–829.
Huang, F.F., Wang, R.C., Xie, L., Zhu, J.C., Erdmann, S., Che, X.D., Zhang, R.Q., 2015. Differentiated rare-element mineralization in an ongonite–topazite composite dike at the xianghualing tin district, southern china: an electron-microprobe study on the evolution from niobium–tantalum-oxides to cassiterite. Ore Geol. Rev. 65 (3), 761–778.
Huang, X.L., Wang, R.C., Chen, X.M., Hu, H., Liu, C.S., 2002. Vertical variations in the mineralogy of the yichun topaz-lepidolite granite, jiangxi province, southern china. Can. Mineral. 40 (4), 1047–1068.
Johan, M.V., Johan, Z., 1994. Accessory minerals of the Cínovec (Zinnwald) granite cupola, Czech Republic Part 1: Nb-, Ta- and Ti-bearing oxides. Mineral. Petrol. 51 (2–4), 323–343.
Johan, Z., Strnad, L., Johan, V., 2012. Evolution of the Cinovec (zinnwald) granite cupola, Czech Republic: composition of feldspars and micas, a clue to the origin of W, Sn mineralization. Can. Mineral. 50 (4), 1131–1148.
Li, J., Huang, X.L., 2013. Mechanism of Ta–Nb enrichment and magmatic evolution in the Yashan granites, Jiangxi Province. South China. Acta Petrol. Sin. 29 (12), 4311–4322 (in Chinese with English abstract).
Li, S., Li, J.K., Chou, I.M., Jiang, L., Ding, X., 2017. The formation of the yichun ta-nb deposit, south china, through fractional crystallization of magma indicated by fluid and silicate melt inclusions. J. Asian Earth Sci. 137 (2017), 180–193.
Linnen, R.L., 1998. The solubility of Nb-Ta-Zr-Hf-W in granitic melts with li and Li +F: constraints for mineralization in rare metal granites and pegmatites. Econ. Geol. 93 (7), 1013–1025.
Linnen, R.L., Cuney, M., 2005. Granite-related rare-element deposits and experimental constraints on Ta-Nb-W-Sn-Zr-Hf mineralization. J. Post Keynesian Econ. 1 (1), 6–15.
Linnen, R.L., Keppler, H., 1997. Columbite solubility in granitic melts: consequences for the enrichment and fractionation of Nb and Ta in the Earth's crust. Contrib. Mineral. Petrol. 128 (2–3), 213–227.
Linnen, R.L., Keppler, H., 2002. Melt composition control of Zr/Hf fractionation in magmatic processes. Geochimica et Cosmochimica Acta 66 (18), 3293–3301.
Liu, Y.S., Hu, Z.C., Gao, S., Günther, D., Xu, J., Gao, C.G., Chen, H.L., 2008. In situ analysis of major and trace elements of anhydrous minerals by la-icp-ms without applying an internal standard. Chem. Geol. 257 (1–2), 34–43.
Manning, D.A.C., 1981. The effect of fluorine on liquidus phase relationships in the system Qz–Ab–Or with excess water at 1 kbar. Contrib. Mineral. Petrol. 76, 206–215.
Monier, G., Robert, J.L., 1986. Evolution of the miscibility gap between muscovite and biotite solid solutions with increasing lithium content: an experimental study in the system K_2O-Li_2O-MgO-FeO-Al_2O_3-SiO_2-H_2O-HF at 600°C, 2 kbar PH_2O: comparison with natural lithium micas. Mineral. Mag. 50, 641–651.
Novák, M., Johan, Z., Škoda, R., Černy, P., Šrein, V., Veselovský, F., 2008. Primary oxide minerals in the system WO_3-Nb_2O_5-TiO_2-Fe_2O_3-FeO and their breakdown products from the pegmatite No.3 at Dolní Bory-Hatě, Czech Republic. Eur. J. Mineral. 20, 487–499.
Novák, M., Černý, P., 1998. Niobium–tantalum oxide minerals from complex granitic pegmatites in the Moldanubicum, Czech Republic: primary versus secondary compositional trends. Can. Mineral. 36, 659–672.
Peng, Z.Z., Wang, S., Ma, Z.S., Yang, G.M., 1988. Crystal structure of Qitianlingite ($Fe_2Nb_2WO_{10}$). Sci. Bull. 33 (10), 856–861.
Qi, L., Hu, J., Gregoire, D.C., 2000. Determination of trace elements in granites by inductively coupled plasma mass spectrometry. Talanta 51 (3), 507–513.
Qiu, R.Z., Deng, J.F., Cai, Z.Y., Zhou, S., Chang, H.L., Du, S.H., 2002. Material sources of granite and ore in Xianghualing mult-metal orefield, Hunan Province. Miner. Deposits 21 (s1), 1045–1048 (in Chinese with English abstract).
Qiu, R.Z., Zhou, S., Chang, H.L., Du, S.H., Beng, S.B., 1998. The evolution of Li-bearing micas from Xianghualing granites and their ore-prospecting significance in Hunan. J. Guilin Inst. Technol. 18 (2), 145–153 (in Chinese with English abstract).
Raimbault, L., Azencott, C., 1987. Géochemie des éléments majeurs et traces du granite á métaux rares de beauvoir. Geologie De La France 2–3, 189–198.
Raimbault, L., Burnol, L., 1998. The Richemont rhyolite dyke, Massif Central, France: a subvolcanic equivalent of rare-metal granites. Can. Mineral. 36 (2), 265–282.
Rao, C., Wang, R.C., Hu, H., Zhang, W.L., 2009. Complex internal textures in oxide minerals from the Nanping No.31 dyke of granitic pegmatite, Fujian province, southeastern China. Can. Mineral. 47, 1195–1212.
Rieder, M., Hybler, J., Smrčok, L., Weiss, Z., 1996. Refinement of the crystal structure of zinnwaldite 2M1. Eur. J. Mineral. 8 (6), 1241–1248.
Schwartz, M.O., 1992. Geochemical criteria for distinguishing magmatic and metasomatic albite-enrichment in granitoids - examples from the Ta-Li granite Yichun (China) and the Sn-W deposit Tikus (Indonesia). Mineralium Deposita 27, 101–108.

Smith, M.P., Henderson, P., Campbell, L.S., 2000. Fractionation of the REE during hydrothermal processes: constraints from the Bayan Obo Fe-REE-Nb deposit, Inner Mongolia, China. Geochimica Et Cosmochimica Acta 64 (18), 3141–3160.
Sun, S.S., Mcdonough, W.F., 1989. Chemical and isotopic systematics of oceanic basalts: implications for mantle composition and processes. Geol. Soc. Lond. Spec. Publ. 42 (1), 313–345.
Sun, T., 2006. A new map showing the distribution of granites in South China and its explanatory notes. Geol. Bull. China 25, 332–335 (in Chinese with English abstract).
Timofeev, A., Migdisov, A.A., Williams-Jones, A.E., 2017. An experimental study of the solubility and speciation of tantalum in fluoride-bearing aqueous solutions at elevated temperature. Geochimica et Cosmochimica Acta 197, 294–304.
Timofeev, A., Williams-Jones, A.E., 2015. The origin of niobium and tantalum mineralization in the Nechalacho REE deposit, NWT, Canada. Econ. Geol. 110, 1719–1735.
Tindle, A.G., Breaks, F.W., 1998. Oxide minerals of the separation rapids rare-element granitic pegmatite group, northwestern Ontario. Can. Mineral. 36 (5), 609–635.
Tindle, A.G., Breaks, F.W., 2000. Columbite-tantalite mineral chemistry from rare-element granitic pegmatites: separation Lakeh area, N.W. Ontario, Canada. Mineral. Petrol. 70 (3–4), 165–198.
Tindle, A.G., Webb, P.C., 1990. Estimation of lithium contents in trioctahedral micas using microprobe data; application to micas from granitic rocks. Chemometrics Intell. Lab. Syst. 29 (5), 148–149.
Tischendorf, G., Gottesmann, B., Forster, H.J., Trumbull, R., 1997. On Li-bearing micas: estimating Li from electron microprobe analyses and an improved diagram for graphical representation. Mineral. Mag. 61, 809–834.
Van Lichtervelde, M., Salvi, S., Beziat, D., Linnen, R.L., 2007. Textural features and chemical evolution in tantalum oxides: Magmatic versus hydrothermal origins for Ta mineralization in the Tanco lower pegmatite, Manitoba, Canada. Econ. Geol. 102, 257–276.
Voloshin, A.V., 1993. Tantalo-niobaty. Sistematika, kristallokhimiya i evolutsiya mineraloobrazovaniya v granitnykh pegmatitakh (Tantalo-Niobates. Systematics, Crystal Chemistry, and Evolution of Mineral Formation in Granitic Pegmatites), St. Petersburg: Nauka.
Wang, R.C., Hu, H., Zhang, A.C., Huang, X.L., Ni, P., 2004. Pollucite and the cesium-dominant analogue of polylithionite as expressions of extreme Cs enrichment in the yichun topaz-lepidolite granite, southern China. Can. Mineral. 42 (3), 883–896.
Wang, Y.M., Duan, J.R., Zhou, C.Z., 1994. The magmatic-diapierc extensional tectonics of Xianghualing, Hunan. Mineral Resour. Geol. 40, 88–92 (in Chinese with English abstract).
Watson, E.B., Harrison, T.M., 1983. Zircon saturation revisited: temperature and composition effects in a variety of crust magma types. Earth Planetary Sci. Lett. 64, 295–304.
Wood, S.A., Samson, I.M., 2000. The hydrothermal geochemistry of tungsten in granitoid environments: I. Relative solubilities of ferberite and scheelite as a function of T, P, pH, and mNaCl. Econ. Geol. 95, 143–182.
Wu, M.Q., Samson, I.M., Zhang, D.H., 2017. Textural and chemical constraints on the formation of disseminated granite-hosted W-Ta-Nb mineralization at the Dajishan Deposit, Nanling Range, Southeastern China. Econ. Geol. 112, 855–887.
Xie, L., Wang, R.C., Che, X.D., Huang, F.F., Erdmann, S., Zhang, W.L., 2016. Tracking magmatic and hydrothermal Nb–Ta–W–Sn fractionation using mineral textures and composition: a case study from the late cretaceous jiepailing ore district in the nanling range in south china. Ore Geol. Rev. 78, 300–321.
Xie, L., Wang, R.C., Groat, L.A., Zhu, J.C., Huang, F.F., Cempírek, J., 2015. A combined empa and LA-ICP-MS study of Li-bearing mica and Sn–Ti oxide minerals from the Qiguling topaz rhyolite (Qitianling District, China): The role of fluorine in origin of tin mineralization. Ore Geol. Rev. 65, 779–792.
Xu, K.Q., Zhu, J.C., 1988. Time–space distribution of tin/tungsten deposits in South China and controlling factors of mineralization. Geol. Tin Deposits Asia Pacific 265–277.
Yin, L., Pollard, P.J., Hu, S., Taylor, R.G., 1995. Geologic and geochemical characteristics of the Yichun Ta-Nb-Li deposit, Jiangxi Province, South China. Econ. Geol. Bull. Soc. Econ. Geol. 90 (3), 577–585.
Yuan, S.D., Peng, J.T., Hu, R.Z., Li, H.M., Shen, N.P., Zhang, D.L., 2008. A precise U-Pb age on cassiterite from the Xianghualing tin-polymetallic deposit (Hunan, South China). Mineralium Deposita 43 (4), 375–382.
Yuan, S.D., Peng, J.T., Shen, N.P., Hu, R.Z., Dai, T.M., 2007. ^{40}Ar-^{39}Ar isotopic dating of the Xianghualing Sn-polymetallic orefield in southern Hunan, China and its geological implications. Acta Geol. Sin (English Edition) 81 (2), 278–286.
Zaraisky, G.P., Korzhinskaya, V., Kotova, N., 2010. Experimental studies of Ta_2O_5 and columbite-tantalite solubility in fluoride solutions from 300° to 550°C and 50 to 100 MPa. Mineral. Petrol. 99, 287–300.
Zhang, W.L., Hua, R.M., Wang, R.C., 2003. Intergrowth of wolframoixiolite and W-rich manganocolumbite in Dajishan tungsten deposit, Jiangxi Province, South China. Mineral Deposits 22 (2), 158–165 (in Chinese with English abstract).
Zhao, L.H., Zou, B.W., Bai, D.Y., 2008. Petrochemical features and tectonic setting of Xianghualing granites in southern Hunan. Geol. Mineral Resour. South China 1, 1–6 (in Chinese with English abstract).
Zhong, J.L., Li, C.P., 2006. Geological characteristics and genesis of Xianghualing skarn type tin deposit. Mineral Resour. Geol. 20 (2), 147–151 (in Chinese with English abstract).
Zhou, X.M., Sun, T., Shen, W.Z., 2006. Petrogenesis of Mesozoic granitoids and volcanic rocks in South China: a response to tectonic evolution. Episodes 29, 26–33.
Zhu, J.C., Wang, R.C., Liu, J.J., Zhang, H., Zhang, W.L., Xie, L., Zhang, R.Q., 2011. Fractionation, evolution, petrogenesis and mineralization of Laiziling Granite Pluton, Southern Hunan Province. Geol. J. China Univ. 17, 381–392 (in Chinese with English abstract).
Zhu, Z.Y., Wang, R.C., Che, X.D., Zhu, J.C., Wei, X.L., Huang, X., 2015. Magmatic–hydrothermal rare-element mineralization in the songshugang granite (northeastern Jiangxi, China): Insights from an electron-microprobe study of Nb–Ta–Zr minerals. Ore Geol. Rev. 65, 749–760.